Journal of Medicinal Chemistry

Article

pubs.acs.org/jmc

Discovery of New Inhibitors of Cdc25B Dual Specificity Phosphatases by Structure-Based Virtual Screening

Antonio Lavecchia,*[,†] Carmen Di Giovanni,[†] Ada Pesapane,[‡] Nunzia Montuori,[‡] Pia Ragno,[§] Nicola Massimiliano Martucci,[∥,⊥] Mariorosario Masullo,[∥,⊥] Emmanuele De Vendittis,[∥] and Ettore Novellino[†]

[†]Dipartimento di Chimica Farmaceutica e Tossicologica, "Drug Discovery" Laboratory, Università di Napoli Federico II, Via Domenico Montesano 49, 80131 Napoli, Italy

[‡]Dipartimento di Biologia e Patologia Cellulare e Molecolare, Università di Napoli Federico II, Via S. Pansini 5, 80131 Napoli, Italy

[§]Dipartimento di Chimica e Biologia, Univeristà di Salerno, Via Ponte don Melillo, 84084 Fisciano (SA), Italy

[∥]Dipartimento di Biochimica e Biotecnologie Mediche, Università di Napoli Federico II, Via S. Pansini 5, 80131 Napoli, Italy

[⊥]Dipartimento di Studi delle Istituzioni e dei Sistemi Territoriali, Università di Napoli "Parthenope", Via Medina 40, 80133 Napoli, Italy

S *Supporting Information*

ABSTRACT: Cell division cycle 25 (Cdc25) proteins are highly conserved dual specificity phosphatases that regulate cyclin-dependent kinases and represent attractive drug targets for anticancer therapies. To discover more potent and diverse inhibitors of Cdc25 biological activity, virtual screening was performed by docking 2.1 million compounds into the Cdc25B active site. An initial subset of top-ranked compounds was selected and assayed, and 15 were found to have enzyme inhibition activity at micromolar concentration. Among these, four structurally diverse inhibitors with a different inhibition profile were found to inhibit human MCF-7, PC-3, and K562 cancer cell proliferation and significantly affect the cell cycle progression. A subsequent hierarchical similarity search with the most active reversible Cdc25B inhibitor found led to the identification of an additional set of 19 ligands, three of which were confirmed as Cdc25B inhibitors with IC_{50} values of 7.9, 4.2, and 9.9 μM, respectively.

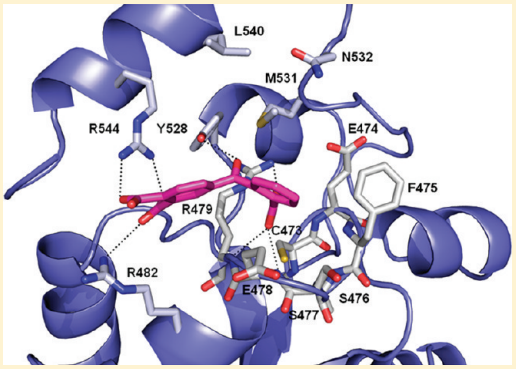

INTRODUCTION

The cyclin-dependent kinases (Cdk) have important functions in the progression of the eukaryotic cell cycle.[1] One of the major mechanisms of cell cycle progression is the regulation of the activities of Cdk1, Cdk2, and Cdk4 by phosphorylation and dephosphorylation. The cell division cycle 25 proteins (Cdc25s) are dual-specificity phosphatases (DSPs) that dephosphorylate conserved threonine and tyrosine residues, thereby activating the Cdk-cyclin complexes, which regulate progression through the cell cycle. Mammalian cells express three Cdc25, Cdc25A, -B, and -C. Cdc25A mainly controls G1/S progression, whereas Cdc25B and Cd25C predominantly activate G2/M transition.[2,3] Mutation analysis has recently revealed that Cdc25A controls both G1/S and G2/M phases and is sufficient for executing a normal cell cycle.[4−7] It is now believed that all three Cdc25 isoforms cooperate to play essential roles in the temporal and spatial regulation of the Cdks during all stages of the cell cycle.[8−11]

Cdc25s have been associated to oncogenic transformation in mice and elevated expression of Cdc25A and Cdc25B at the mRNA and/or protein level has been reported in a wide variety of primary human tumors with poor prognosis such as breast cancer,[12] colon cancer,[13] non-Hodgkin's lymphoma,[14] prostate cancer,[15] pancreatic ductal adenocarcinoma,[16] and lung cancer.[17] Enhanced expression of Cdc25A and Cdc25B in tumors correlates with specific clinical and pathological features: higher-grade or later-stage tumors, more aggressive tumors, and a shorter disease-free survival.[8,9] Recent findings described the involvement of Cdc25A in the adhesion-dependent proliferation of acute myeloid leukemia cells.[18] The inhibition of Cdc25 phosphatases may thus represent a novel approach for the development of anticancer therapeutics.

The crystal structure of the ligand-free form of catalytic domain of Cdc25A (PDB ID: 1C25)[19] and Cdc25B (PDB ID: 1QB0)[20] has been solved at 2.3 Å and 1.9 Å resolution, respectively. Both phosphatases contain the conserved HCX_5R protein tyrosine phosphatase catalytic-site motif, which can be superimposed with all other active site loops in protein tyrosine phosphatases (PTPs) with known structures.[10,11] Although the overall structure of the catalytic domains of the two Cdc25 phosphatases is similar, key differences in the positions of some

Received: October 7, 2011
Published: April 23, 2012

 © 2012 American Chemical Society

residues believed to be essential for catalysis have been identified. For example, the carbonyl backbone of residue 434 in Cdc25A (residue 477 in Cdc25B) points toward the region where the phosphate should accommodate, which is the opposite of that observed with Cdc25B and other PTPs. In addition, E431 side chain in Cdc25A points into the catalytic site, narrowing the cavity in opposition to the corresponding E474 side chain residue in Cdc25B.[19] Another important difference involves the location of the side chain for R436 in Cdc25A, which appears to be misplaced when compared to the structures of the Cdc25B catalytic domain and other known phosphatases. Cdc25A fails to bind oxyanions in its catalytic site, whereas Cdc25B readily binds tungstate and sulfate in a way similar to other PTPs and DSPs. The other diversities between the Cdc25B and Cdc25A catalytic domains reside in the C-terminal region (residues 531−547, Cdc25B numbering). This region of Cdc25B, which is well ordered in the crystal structure, contains an α-helix that is positioned against the bulk of the protein, in the region exposed to the solvent. Some residues of the helix, such as M531 and R544, point toward the active-site cleft, whereas in the Cdc25A core structure this region is undefined. Thus, the active-site region of Cdc25A is maintained in a flat conformation and exposed to bulk solvent, whereas the structure of the catalytic domain of Cdc25B reveals a shallow and small active site, located next to a large cavity, defined as a "swimming pool" by Rudolph[21] for the many well-organized water molecules contained (Figure 1).

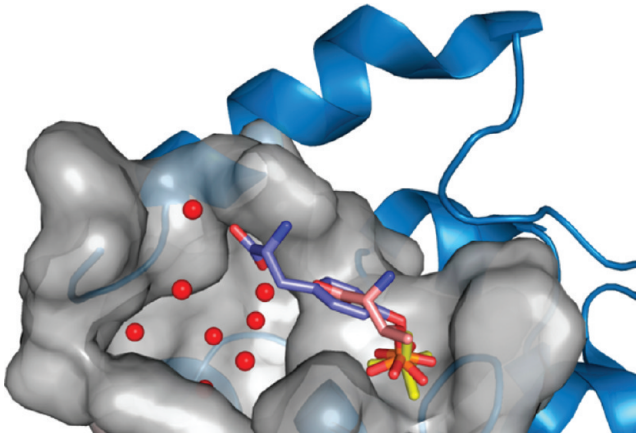

Figure 1. Control docking results. The lowest energy docked positions of phosphothreonine (pink) and phosphotyrosine (light-blue) are shown as stick representations surrounded by a blue ribbon model of Cdc25B (1QB0). The catalytic site and the adjacent deeper and larger "swimming pool" pocket containing several water molecules in red are displayed as light-gray Connolly surface. For the ligands, oxygen is red, nitrogen blue, and phosphorus orange. The crystallographic sulfate is shown in yellow.

Over the past few years, several synthetic and natural molecules with different structural features targeting Cdc25 activity have been reported.[10,22,23] Their structures are reported in Chart 1. The most potent ones share the *para*-quinone moiety such as the thio-ether derivative Cpd 5, which inhibits Cdc25 activity in Hep3B cells[24] or NSC-95397 which blocks cell cycle at the G2/M transition.[25] Adociaquinone B is a natural product isolated from a marine sponge that inhibits in vitro Cdc25B activity with an IC_{50} value of 70 nM.[26] More recently, BN-82685 was demonstrated to inhibit in vivo the growth of human pancreatic MiaPaCa2 tumors xenografted on athymic nude mice.[27] IRC-083864 containing two quinone nuclei is the most potent Cdc25 inhibitor with an IC_{50} value of ~20 nM, which also exhibits antiproliferative properties against MiaPaCa2 and LNCaP cell lines and xenografted tumors.[28]

Binding modes of the newly found Cdc25 inhibitors have also been addressed with docking simulations in the active site to gain structural insight on the inhibitory mechanisms.[25,29,30]

Many of these molecules contain reactive groups and can, for example, covalently modify the catalytic cysteine residue (C473) through sulfhydryl arylation or could form an ether linkage with serine residues. Moreover, the redox properties of the quinones can also potentially generate toxic oxygen species.[31,32] Redox cycling and oxidative stress are initiated by the single electron reduction of quinones by NADH-cytochrome P450 oxidoreductase, NADH-cytochrome b5 oxidoreductase, and NADH-ubiquinone oxidoreductase.[33] This may cause toxicity to normal tissue, thus reducing the therapeutic usage of these molecules. This suggests that novel inhibitors lacking such reactive groups would be very valuable to assist in the development of new antineoplastic agents.

Here we report the discovery of small molecule inhibitors of Cdc25 phosphatase activity. These molecules were identified by a combination of experimental and virtual screenings of both National Cancer Institute (NCI) Diversity Set and ZINC[34] databases. We identified molecules that inactivate/inhibit Cdc25B at micromolar concentration in vitro, inhibit breast (MCF-7), prostate (PC-3), and leukemia (K562) cancer cell proliferation, and significantly affect the cell cycle progression.

RESULTS

Validation of the Docking Method. Initial docking calculations were performed using phosphorylated amino acid substrates to evaluate Cdc25B as a structural model for virtual screening as well as to test the performance of the GLIDE[35] docking and scoring. Phosphothreonine and phosphotyrosine were docked to the Cdc25B active site. GLIDE determined similar binding positions for both compounds, with lowest predicted GLIDE XP scores of −6.70 and −6.26 kcal/mol for phosphothreonine and phosphotyrosine, respectively. The calculated structural determinants of the phosphate group of these compounds matched well with the location of a free sulfate molecule observed in the Cdc25B crystal structure[20] (Figure 1) that should mimic the incoming phosphate group of the substrate.

Identification of Lead Compounds Using GLIDE with the NCI Diversity Set and ZINC Databases. Following the success of the control dockings, virtual screening calculations were performed with the Cdc25B crystal structure model, using a database of compound structures from the NCI Diversity Set and ZINC. The distribution of the GLIDE XP scores for the best-ranked 128 compounds from the NCI Diversity Set and the best-ranked 80 compounds from the ZINC database is shown in Figure 2.

The NCI Diversity Set delivers many significantly lower XP Gscores that likely result in more potent inhibitors. The average molecular weight for the best-scoring 128 compounds from the NCI Diversity Set is 237.8; the corresponding value for the best 80 ZINC-compounds is 234.8. The complexes for the best-ranked 128 compounds from the NCI Diversity Set resulting from the XP processing and the best-ranked 80 XP hits from the ZINC database were submitted to display and visual inspection. Many well-ranked structures were considered unlikely, as they display poor conformations including twisted

dx.doi.org/10.1021/jm201624h | J. Med. Chem. 2012, 55, 4142−4158

Chart 1. Known Cdc25 Inhibitors

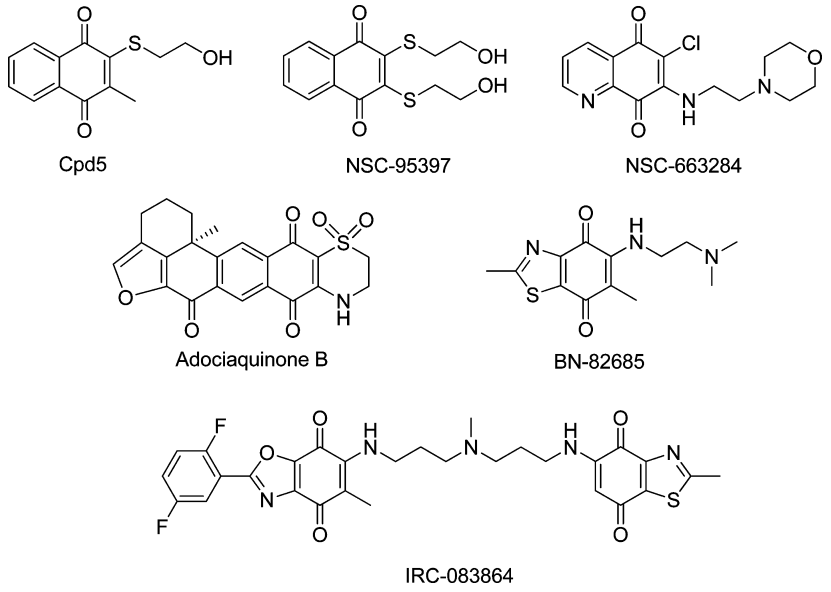

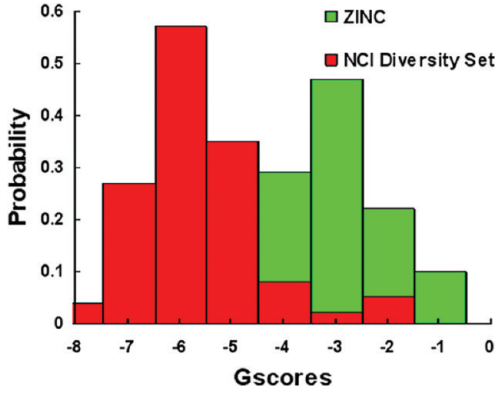

Figure 2. Distributions of the GLIDE XP scores for the best-ranked 128 NCI Diversity Set (red bars) and the best-ranked 80 ZINC (green bars) compounds.

amide and ester groups or overlay short nonbonded contacts. Three primary binding modes were observed: ligands bound to either one of the two binding sites (catalytic or adjacent "swimming pool") as well as to the connection area joining these two cavities. A larger number of hits were found to bind to the catalytic site rather than to the "swimming pool". Final selection of compounds also took into account chemical diversity, properties predicted by the QikProp program,[36] and QikProp alerts concerning potentially undesirable chemical substructures. Structural diversity in compound selection is desired to provide alternative lead series for optimization. Ultimately, 23 compounds from NCI Diversity Set and seven compounds from the ZINC database were selected for in vitro testing (Figure 3).

Before biochemical evaluation, these hits were inspected on a large electronic collection of organic chemistry (CrossFire Beilstein) using the MDL CrossFire Commander.[37] Additional searches were performed using the PubChem compound database,[38] a publicly available source of chemical and biological information for small molecules, including results from NCI anticancer drug screenings. Of utmost importance was the finding that none of the 30 selected compounds had been previously tested as a Cdc25 inhibitor.

In Vitro Assay of Inhibition Activity. The selection of compounds for further analysis was based on an in vitro Cdc25B inhibition assay in which the cutoff was set so that a compound with at least 30% inhibition at 100 μM was defined as active. According to these criteria, 15 active compounds were identified; their percent of inhibition on Cdc25A, -B, and -C activity is reported in Table 1. Compounds **5**, **11**, and **19** exhibited the highest percentage of inhibition of Cdc25A and -B activity. In particular, compounds **5** and **11** showed a ~100% inhibition of Cdc25A, -B, or -C activity, whereas compound **19** showed a ~80% inhibition of both Cdc25A and -B and a 63% inhibition of Cdc25C.

To assess the reversibility of Cdc25 phosphatase inhibitors, we used a dilution method described previously.[39] Briefly, Cdc25B was preincubated for 20 min with the different inhibitors (100 μM) or with DMSO, as a vehicle control; after a 10-fold dilution of the incubation mixture, the residual enzyme activity was measured. The data reported in Figure 4 show that compounds **5** and **11** led to a complete inhibition of Cdc25B activity. Therefore, the lack of functional recovery after the 10-fold dilution suggests that these molecules act as irreversible inhibitors. In contrast, the enzyme activity was almost completely restored in the presence of compounds **7**, **12**, **13**, **16**, **20**, **21**, **23**, and **27**, so they were classified as reversible inhibitors (Figure 4). An intermediate behavior was observed with compounds **6**, **8**, **18**, **19**, and **22** because the enzyme activity was only partially restored upon dilution. Therefore, we selected for further in vivo studies compound **11** [3-(4,5,6-trihydroxy-3-oxo-3*H*-xanthen-9-yl)propanoic acid], as a Cdc25B irreversible inhibitor, compound **12** [5-((2-hydroxy-4-methylquinolin-6-yl)methyl)-2-methoxybenzenesulfonic acid], as a Cdc25B reversible inhibitor, and compounds **18** [5,5′-(3-(pyridin-2-yl)-1,2,4-triazine-5,6-diyl)difuran-2-sulfonic acid] and **19** [4-(2-carboxybenzoyl)phthalic acid], as two Cdc25B inhibitors with intermediate behavior.

Kinetic Studies. The inhibition mechanism of the selected compounds was further investigated through kinetic studies to evaluate the effect of the different inhibitors on the phosphatase activity of a purified recombinant form of Cdc25B catalytic domain. In a first approach to define the inhibition power of

dx.doi.org/10.1021/jm201624h | *J. Med. Chem.* 2012, 55, 4142–4158

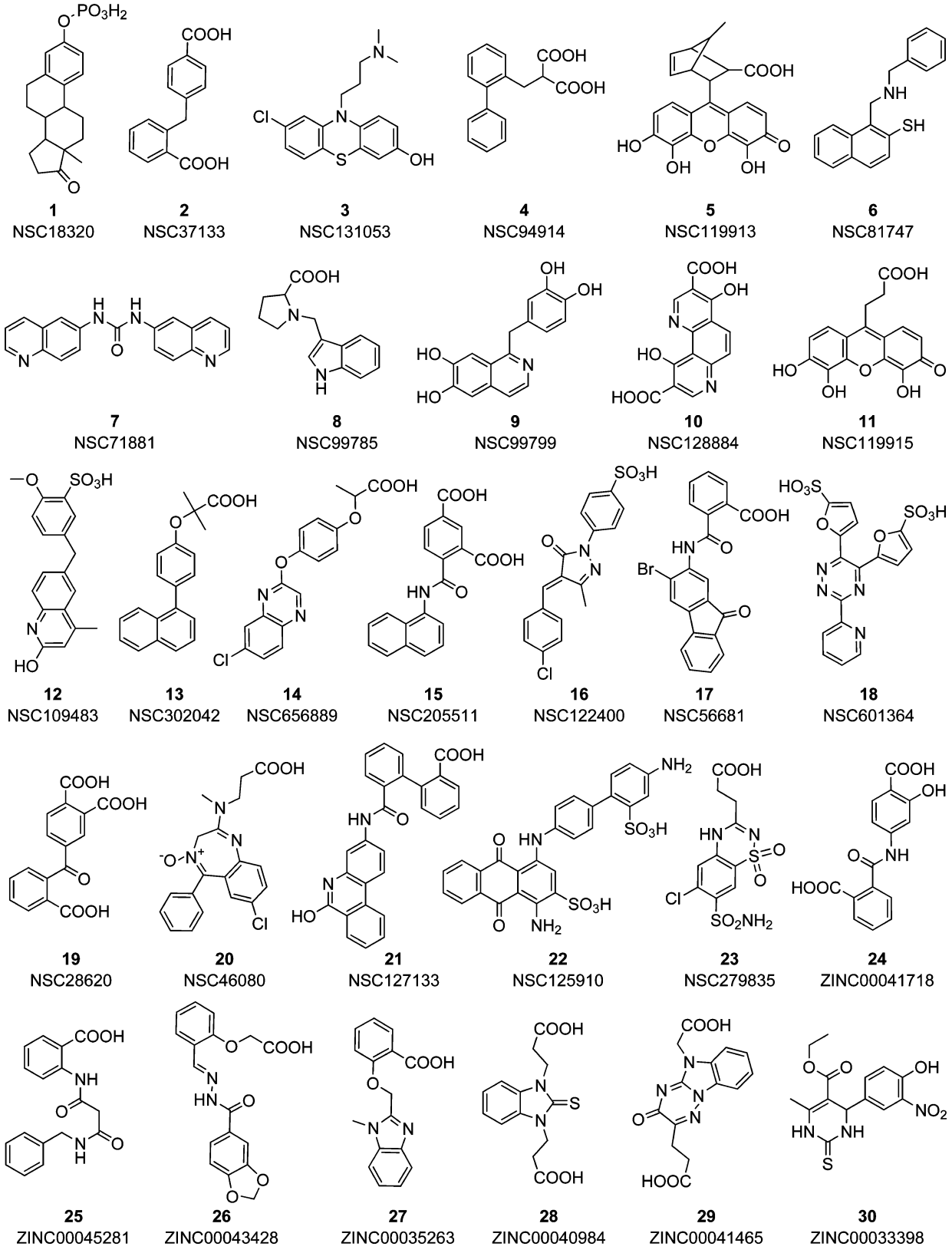

Figure 3. Chemical structures of compounds selected from NCI Diversity Set (**1**–**23**) and ZINC library (**24**–**30**) identified from virtual screening.

each compound, a fixed 25 μM concentration of the synthetic substrate 3-*O*-methyl fluorescein phosphate (OMFP) was used and its hydrolysis rate by 10 nM Cdc25B was measured as a function of inhibitor concentration. As reported in Figure 5, the highest inhibition power was measured with compound **11**, which led to the complete loss of activity in a narrow range of inhibitor concentration; the estimated IC_{50} value for this molecule was 0.10 μM (Table 2). Interestingly, an almost overlapping inhibition profile was obtained when the effect of this compound was determined either on a 10-fold diluted

dx.doi.org/10.1021/jm201624h | *J. Med. Chem.* 2012, 55, 4142–4158

Table 1. Properties of the Selected Cdc25 Inhibitors[a]

	% inhibition at 100 μM				
compd	Cdc25A	Cdc25B	Cdc25C	GLIDE XP score	XP rank
5	98	98	98	−7.14	13
6	35	60	53	−6.01	41
7	47	32	48	−3.44	58
8	39	37	45	−6.59	42
11	100	99	99	−6.24	8
12	46	41	55	−6.06	2
13	47	40	50	−5.29	8
16	17	46	54	−5.08	5
18	41	53	35	−4.95	7
19	80	80	63	−5.36	56
20	28	43	48	−3.61	7
21	66	45	48	−5.42	21
22	72	89	49	−3.06	1
23	21	41	47	−5.59	33
27	10	43	35	−3.95	24
vanadate	77	91	90		

[a]Percent of inhibition of Cdc25A, -B, and -C phosphatase activity, GLIDE XP scores and rankings for compounds selected from the NCI Diversity Set and ZINC databases were obtained as described in the Experimental Section.

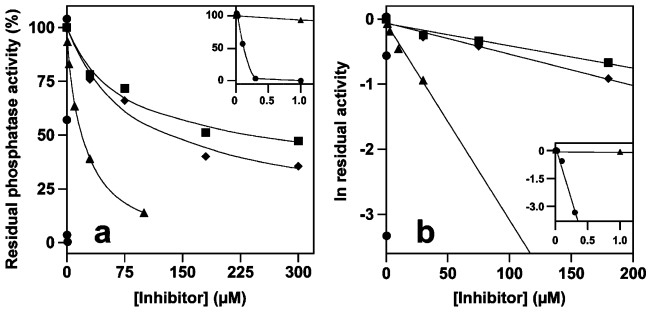

Figure 5. Dose-dependent inhibition profile by the selected Cdc25B inhibitors. The phosphatase activity of 10 nM Cdc25B was measured through the rate of OMFP hydrolysis in the presence of 25 μM substrate and the indicated concentration of **11** (circles), **12** (diamonds), **18** (squares), or **19** (triangles). A close-up at low inhibitor concentration is reported in the inset. The activity was expressed either as a percentage of that measured in the absence of inhibitor (a) or as a natural logarithm of the ratio of residual activity (b); in this second case, the highest concentration of each inhibitor was not considered in the representation of the data. Other details are described in the Experimental Section.

mixture containing enzyme and inhibitor or when dithiothreitol (DTT) was omitted in the reaction mixture (data not shown). A typical inhibition profile was instead observed with compound **19** (Figure 5), which followed the classical dose-dependent response; the calculated IC_{50} for this molecule was 17.5 μM (Table 2). A significantly lower inhibition was found with compounds **12** and **18** (Figure 5), for which the estimated IC_{50} was higher than 100 μM (Table 2).

To prove the effect of the selected compounds on other members of the Cdc25 family, their inhibition power was tested on a purified recombinant form of Cdc25A catalytic domain. All tested compounds inhibited the phosphatase activity of Cdc25A (Supporting Information Figure S1) and the calculated IC_{50} values are reported in Table 2. No great differences emerged when comparing these data with those obtained for Cdc25B inhibition. In particular, also in this case the greatest effectiveness in the inhibition of Cdc25A was observed with compound **11**; a lower inhibition was measured with the other inhibitors, and **19** was by far more effective than **12** and **18**.

To get an insight in the type of inhibition exerted by the different molecules and to measure their K_i values through kinetic measurements, the affinity of Cdc25B for OMFP was measured either in the absence or in the presence of fixed inhibitor concentrations. The corresponding Lineweaver–Burk plots obtained for each compound are presented in Figure 6.

The results related to compound **11** indicate that this molecule reduced the maximum rate of OMFP hydrolysis, without affecting the K_M for OMFP (Figure 6a). From these data, it could be inferred that compound **11** acted as an irreversible inhibitor of Cdc25B with a calculated K_i of 0.08 μM (Table 2). Under this concern, it has been reported that quinonoid inhibitors could act on enzyme members of the Cdc25 family through the formation of reactive oxygen species (ROS), a finding based on the observation that their inhibiton power was attenuated by ROS scavengers added in the reaction

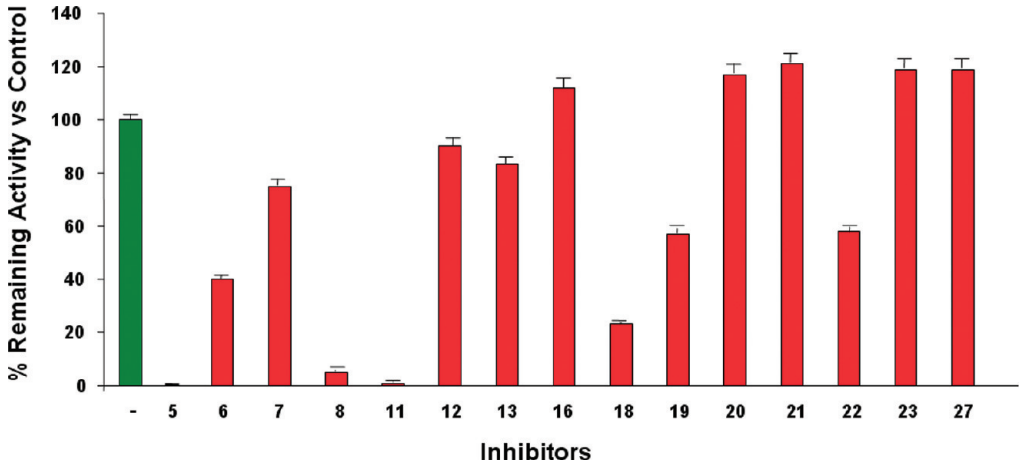

Figure 4. Reversibility of Cdc25B inhibition by the selected compounds. Cdc25B (0.5 μg) was incubated for 20 min at room temperature with 100 μM of the indicated inhibitors or DMSO as a vehicle control. Following a 10-fold dilution, the residual activity was measured as reported in the Experimental Section, upon addition of OMFP. Results are expressed as a percent of residual activity (red bars) vs untreated control (green bar) and represent the averages ± SD of three different determinations.

dx.doi.org/10.1021/jm201624h | J. Med. Chem. 2012, 55, 4142–4158

Table 2. Predicted Properties of Selected Cdc25 Inhibitors from QikProp and Values of IC_{50} and K_i for the Inhibition of Cdc25A and Cdc25B

						Cdc25A		Cdc25B	
compd	MW[a]	QP log P[b]	QP log S[c]	QP P_{Caco}[d]	no. of primary metabolites[e]	IC_{50}[f] (μM)	K_i[f] (μM)	IC_{50}[f] (μM)	K_i[f] (μM)
11	316.3	0.45	−2.66	3	5	0.24 ± 0.03	0.07 ± 0.01	0.10 ± 0.01	0.08 ± 0.04
12	359.4	2.88	−4.29	32	4	86 ± 13	203 ± 75	133 ± 6	84 ± 23
18	474.4	0.57	−2.48	1	3	110 ± 15	139 ± 50	173 ± 97	159 ± 66
19	314.3	1.27	−2.67	0	none	6.0 ± 1.2	2.3 ± 0.3	17.5 ± 5.0	5.3 ± 2.4

[a]Molecular weight, range 95% of drugs (130/725). [b]Predicted octanol/water log P, range 95% of drugs (−2/6.5). [c]Predicted aqueous solubility, S, in mol/L, range 95% of drugs (−6.5/0.5). [d]Predicted Caco-2 cell permeability in nm/s, range 95% of drugs (<25 poor, >500 great). [e]Range 95% of drugs (1/8). [f]IC_{50} and K_i were calculated as described in the Experimental Section. Results represent averages ± SD of three different determinations.

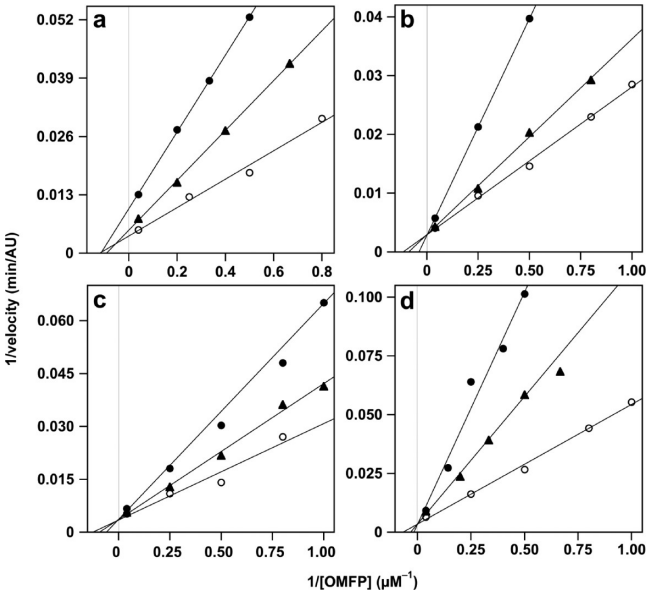

Figure 6. Effect of the selected inhibitors on the Lineweaver−Burk plots of the Cdc25B phosphatase activity. The phosphatase activity was measured through the rate of OMFP hydrolysis by 10 nM Cdc25B in the presence of 1−25 μM OMFP. The activity was determined either in the absence (empty circles) or in the presence of fixed inhibitor concentrations (filled symbols); in particular, the concentration of inhibitor was 0.05 μM (triangles) or 0.1 μM (circles) for **11** (a); 30 μM (triangles) or 100 μM (circles) for **12** (b) or **18** (c); 10 μM (triangles) or 20 μM (circles) for **19** (d), respectively. Other details are described in the Experimental Section.

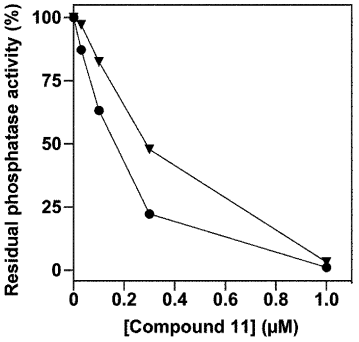

Figure 7. Effect of superoxide dismutase on the dose-dependent inhibition profile of Cdc25B by compound **11**. The phosphatase activity of 10 nM Cdc25B was measured as reported in Figure 6 in the absence (circles) or in the presence (reverse triangles) of 2 nM recombinant superoxide dismutase from *Helicobacter pylori* corresponding to 0.12 Units. Other details are described in the Experimental Section.

mixture; a direct oxidation of the enzyme by the ROS likely formed during the enzyme−inhibitor interaction was proposed.[40−42] For this reason, we checked if a ROS scavenger, such as the purified recombinant form of superoxide dismutase from *Helicobacter pylori* (*Hp*SOD) (unpublished result) could affect the inhibition of Cdc25B by compound **11**. Interestingly, while *Hp*SOD had no effect on the activity of Cdc25B in the absence of the inhibitor, the ROS scavenger significantly attenuated the inhibition power of **11** (Figure 7); the calculated IC_{50} for this compound in the presence of *Hp*SOD increased to 0.33 μM.

Additional information on the effect of **11** on Cdc25B derived from SDS/PAGE analysis. In particular, we verified if compound **11** caused a dose- and time-dependent variation of the protein content in Cdc25B solutions treated with this inhibitor. To this aim, 3.9 μM solutions of this enzyme were incubated in the absence or in the presence of 4, 40, or 400 μM compound **11** and then analyzed by SDS/PAGE at different times (Supporting Information Figure S2). The inhibitor caused a marked reduction of the amount of Cdc25B after 1 h treatment with the highest concentration of the inhibitor. Furthermore, a 30 min incubation of Cdc25B (2.1 μM) with increasing concentration of **11** (4, 40, or 400 μM) caused a dose-dependent decrease of the enzyme content in the solution (Supporting Information Figure S3). These results suggest that **11** caused a precipitation of the enzyme when the inhibitor was present at high concentrations, probably reflecting the tendency of Cdc25B to form protein aggregates due to the oxidative environment formed in the presence of the inhibitor. This hypothesis was also confirmed in a Cdc25B sample purified in the absence of reducing agents. Indeed, the ESI-Q/TOF MS analysis, carried out on the protein precipitate obtained at the end of the purification procedure, revealed the presence of oligomeric forms of the enzyme (data not shown).

When considering the type of inhibition observed with the other selected compounds, a different feature emerged for compound **19**. Indeed, in the presence of this compound an increase in the K_M for the substrate was observed, without any variation of the maximum rate of OMFP hydrolysis, a typical behavior for a reversible competitive inhibitor of Cdc25B (Figure 6d). The value of K_i obtained for compound **19** was 5.3 μM (Table 2). The behavior of both **12** (Figure 6b) and **18** (Figure 6c) was similar to **19**, thus suggesting that also these molecules act as reversible competitive inhibitors of Cdc25B, although their K_i values were significantly higher. Indeed, the K_i obtained for **12** and **18** was 84 and 159 μM, respectively (Table 2).

dx.doi.org/10.1021/jm201624h | J. Med. Chem. 2012, 55, 4142−4158

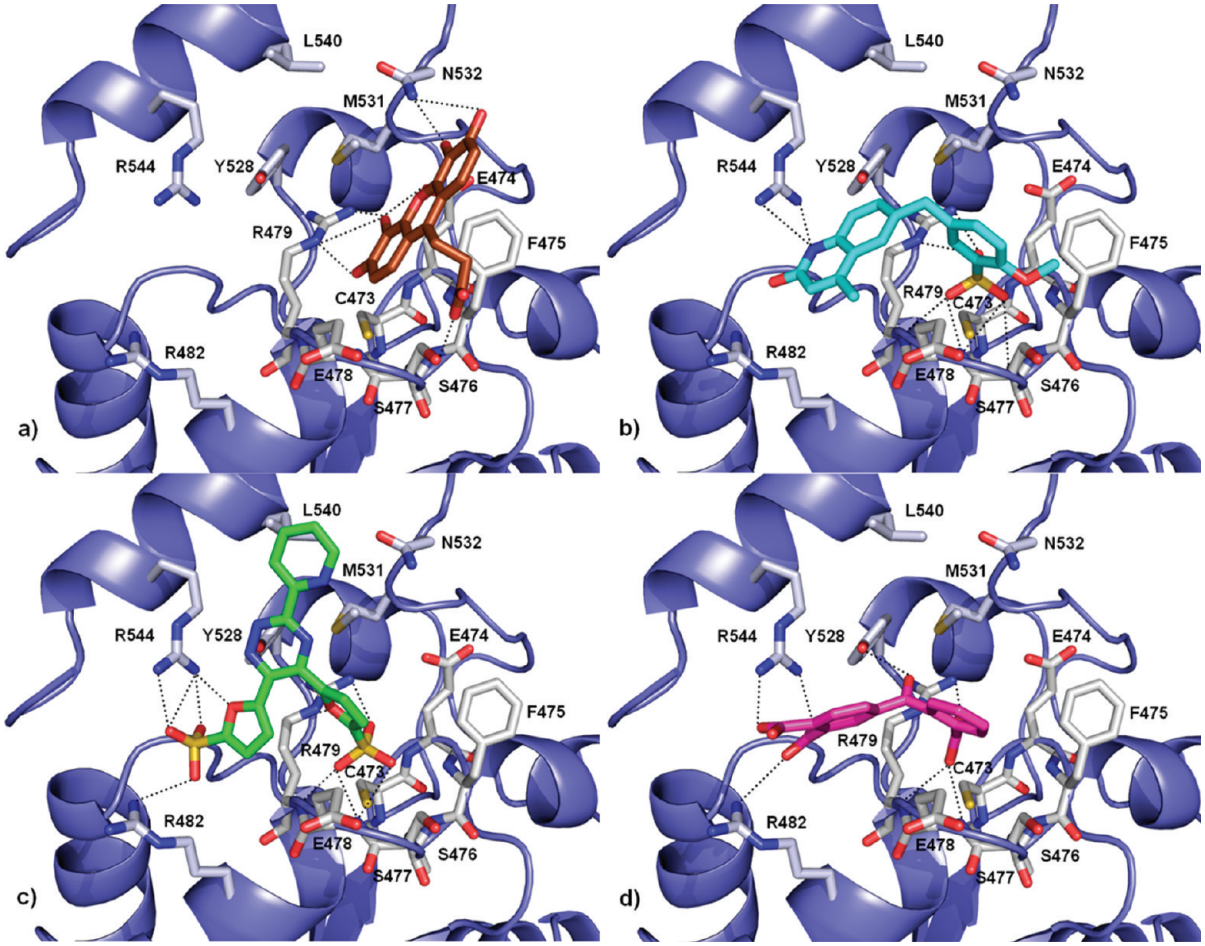

Figure 8. Binding modes of compounds **11** (a, brown), **12** (b, cyan), **18** (c, green), and **19** (d, magenta) in the Cdc25B binding cavity as calculated by GLIDE. For clarity, only interacting residues are displayed and labeled. Ligands and interacting key residues (white) are represented as stick models, while the protein is a sky-blue ribbon model. H-bonds and salt bridges are shown as dashed black lines.

The K_i values for the selected compounds were also determined toward the Cdc25A phosphatase activity, and the results are reported in Table 2. Also in this case no great differences emerged in comparison with Cdc25B, thus confirming that compound **11** had the greatest effectiveness and that, among the other inhibitors, **19** was by far more effective than **12** and **18**.

Structural Basis for Cdc25B Inhibition by Compounds 11, 12, 18, and 19. To obtain a structural insight into the mechanisms by the newly identified Cdc25B inhibitors **11**, **12**, **18**, and **19**, their binding modes in the active site of Cdc25B were investigated using the GLIDE program[35] with the procedure described in the Experimental Section. Figure 8 depicts the predicted binding modes of the four inhibitors in the active site of Cdc25B. All the top-ranked poses place ligands at the junction between the catalytic pocket and the "swimming pool", with the exception of **11**, which binds only to the catalytic pocket.

Under physiological conditions, compound **11** exhibits ionization as well as prototropic tautomerism: it forms two different skeleton tautomers, the 3-(4,5-dihydroxy-6-oxido-3-oxo-3*H*-xanthen-9-yl)propanoate (**11a**) and the (*E*)-3-(3,4,5-trihydroxy-6-oxido-9*H*-xanthen-9-ylidene)propanoate (**11b**), which are mainly in the dianionic form at neutral pH (Scheme 1). Ligand tautomers and ionization species in aqueous solution were estimated for water under the conditions of experiments

Scheme 1. Tautomer and Ionization Equilibria of Compound 11

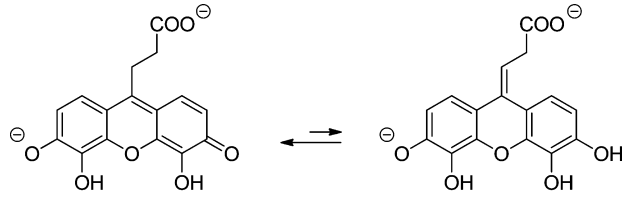

(pH 7.5 and 30 °C), using the SPARC[43] online calculator. Density functional theory (DFT) calculations showed that the difference between the solution-phase free energies of the two tautomeric forms was large enough (−41.2 kJ/mol) in favor of the **11a** tautomer over the **11b** one to justify the dominating presence of the former in an equilibrium situation. This is in consonance with the results previously reported for the keto−enol equilibrium of a similar xanthenone compound, the 6-hydroxy-9-(hydroxymethyl)-3*H*-xanthen-3-one.[44]

As illustrated in Figure 8a, the top-scoring solution predicted by GLIDE for **11** extends deep into the catalytic site of Cdc25B, making several H-bonds and hydrophobic interactions with key residues of the catalytic site. In particular, the 3-quinone carbonyl oxygen and the adjacent 4-OH group form H-bonds with both the R479 and E474 side chains, whereas the

dx.doi.org/10.1021/jm201624h | *J. Med. Chem.* 2012, 55, 4142−4158

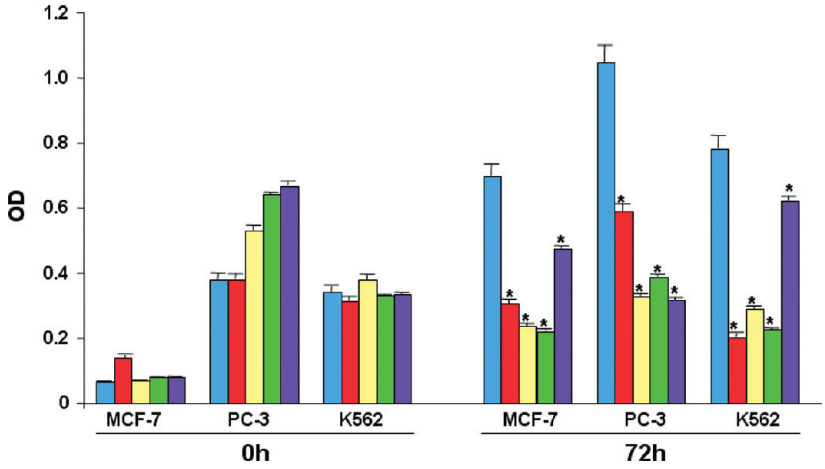

Figure 9. (a) Growth inhibitory effects of compounds **11** (red bars), **12** (yellow bars), **18** (green bars), and **19** (purple bars) on human cancer cells. MCF-7, PC-3, and K562 cells were treated with selected inhibitors or with DMSO (blue bar), as a vehicle control. The values obtained at the indicated times represent the mean ± SD of three experiments. (*) $p \leq 0.05$, as determined by the Student's t test.

nondissociated and dissociated OH groups at positions 5 and 6 of the xanthenyl ring system establish H-bonds with N532 residue. Moreover, the propanoic acid side chain engages a H-bond with the catalytic S477 OH group. Finally, the xanthenyl group forms van der Waals interactions with the phenyl ring of F475 and M531. Recent evidence suggested that some quinones can act as inhibitors of the Cdc25B phosphatase by promoting a covalent modification of the enzyme or by oxidizing and inactivating the catalytic cysteine of the enzyme through redox cycling and/or production of ROS.[40−42] The covalent modification of the enzyme can be ascribed to different nucleophilic entities such as cysteines, serines, or arginines present in the catalytic site. The proposed binding orientation of **11** into the Cdc25B active site can support all the proposed mechanisms of action.

As depicted in Figure 8d, the carboxylate group of the benzoyl moiety of the most active reversible inhibitor **19** binds deep in the active site pocket of Cdc25B, similar to the binding of a natural pTyr substrate, while the two carboxylate groups of the phthalic moiety bind in the "swimming pool". In particular, the first carboxylate makes a salt-bridge with the R479 guanidinium group and engages a H-bond with the catalytic backbone NHs of R479 and E478. The two carboxylates form salt-bridges with both R482 and R544 side chains within the "swimming pool". The carbonyl group of the inhibitor also accepts a H-bond from the Y528 OH group. The binding orientation, as suggested by GLIDE, shows that the carboxylate group of the benzoyl moiety in **19** approximates the binding mode of the sulfate ion bound to the catalytic site of the Cdc25B crystal structure and, consequently, many of the interactions seen between the sulfate ion and the phosphate-binding loop in Cdc25B structure are conserved between Cdc25B and **19**. The observed competitive inhibition pattern of **19** corroborates this proposed orientation and suggests that the carboxylate linked to aromatic ring can also serve as a nonphosphorous-containing pTyr mimicking compound.

GLIDE predicted comparable solutions for reversible inhibitors **12** (Figure 8b) and **18** (Figure 8c). In particular, the sulfonate group of **12** undergoes multiple H-bond interactions with the catalytic backbone NHs of R479, E478, and S477 and forms a salt bridge with the guanidinium group of R479. The nitrogen of the quinolin-2-ol moiety forms a bifurcated H-bond with the guanidinium group of R544 within the "swimming pool". Modeling also indicated that both aromatic and quinolin-2-ol rings of **12** make van der Waals interactions with side chain carbon atoms of E478, R479, and M531. A similar binding mode was also found for compound **18**, which occupies both the active site and the "swimming pool" as well as the connection area in between these two cavities. The sulfonate group of one furan ring projects toward the catalytic pocket, establishing analogous H-bonds and electrostatic interactions with the catalytic backbone NHs, as also found for **12**. The sulfonate group of the second furan ring together with the furan oxygen is held within the "swimming pool" by salt-bridges and H-bonds with both R482 and R544 side chains. In addition, the pyridine ring makes hydrophobic contacts with L540 and M531.

The identification of compounds **12** and **18** as potential Cdc25B inhibitors from the GLIDE screening was not surprising because aryl sulfonic acids are structural analogues of aryl phosphonic acids. The structural similarity of aryl sulfonate moieties to pTyr and the GLIDE predicted modes of binding for **12** and **18**, in which the aryl sulfonate moieties approximate the interactions between the sulfate ion and the active site of Cdc25B, could explain the competitive inhibition pattern observed for **12** and **18**. It was also demonstrated that suramin, a hexasulfonated polyaromatic naphthylurea, and several polysulfonic derivatives of suramin that contain multiple naphthylsulfonic acid groups or phenylsulfonic acid groups, are also competitive, reversible Cdc25 inhibitors.[45] Thus, the fact that **12** and **18** were identified from the active site-targeted GLIDE and competitively inhibited Cdc25B validates the docking approach.

To gain structural insights into the inhibitory mechanism of the most active inhibitors **11** and **19** for Cdc25A, docking simulations were also carried out in the active site of a homology-modeled structure of Cdc25A.[46] As depicted in Figure S4 of Supporting Information, the two ligands bind in the active site of Cdc25A in a similar fashion to that observed in Cdc25B, forming the same pattern of interactions. The high homology (sequence identity, 66.7%; similarity, 76.5%) between Cdc25A and Cdc25B includes nearly identical phosphate binding sites and hence similar binding pockets for inhibitors, with only few amino acids that differ between the two phosphatases. Specifically, residue M403, located near the active site of Cdc25A, replaces the corresponding L445 in

Cdc25B (this position is not shown in Figure S4 of Supporting Information) and H489, at the top of the active site, replaces N532. Other residues differing between Cdc25A and Cdc25B in the vicinity of the phosphate binding site are generally considered too remote to significantly influence the binding of inhibitors with "drug-like" molecular weight or are oriented with their side chains away from the cleft itself. This helps to explain why compounds **11** and **19** do not show significant selectivity against the two isoenzymes.

Effects of Cdc25 Phosphatase Inhibitors on Cell Proliferation and Cell Cycle Progression. The Cdc25 phosphatase family has a central role in controlling cell proliferation and cell cycle progression; therefore, we evaluated the effects of compounds **11**, **12**, **18**, and **19** on the growth of breast (MCF-7), prostate (PC-3), and leukemia (K562) cancer cell lines, expressing Cdc25A, -B, and -C.[47−49] All compounds were able to significantly reduce cell viability after 72 h of treatment (Figure 9), although with a different efficacy; indeed, while compound **11** was active at 20 μM concentration, compound **19** exerted its effect at 200 μM concentration and compounds **12** and **18** at 400 μM concentration.

In addition, we investigated whether the effect of compound **11** on cell proliferation could also depend on ROS generation. To this aim, the cell-permeable ROS indicator, H_2DCFDA, was used to detect by flow cytometry analysis intracellular oxidation in K562 cells exposed to **11** with or without pretreatment with DTT. DTT is a strong reducing agent that is often used to promote a cellular reductive stress. It can cross membranes and shift the redox balance of important biological redox couples, such as the NAD^+/NADH, $NADP^+$/NADPH, and GSSG/GSH couples, to a more reducing state. As shown in Figure 10,

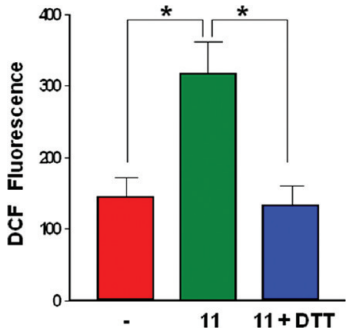

Figure 10. Effect of quinonoid compound **11** on cellular ROS formation. Intracellular oxidation of H_2DCFDA-loaded untreated K562 cells (−), **11**-only treated K562 cells (**11**), or K562 cells preincubated with 1 mM DTT and then treated with **11** (**11**+DTT) was analyzed by flow cytometry. Bars indicate the mean ± SEM of three different experiments. (*) $p \leq 0.05$, as determined by the Student's *t* test.

cellular ROS content increased after treatment with 20 μM compound **11** for 30 min, as compared to untreated cells (mean fluorescence intensity ± SEM of three different experiments: 316.7 ± 43.6 vs 144.0 ± 27.0; $p < 0.05$). Moreover, cell treatment with 1 mM DTT, before the addition of **11**, decreased the cellular ROS content as compared to **11**-only treated cells (mean fluorescence intensity ± SEM of three different experiments: 132.3 ± 27.2 vs 316.7 ± 43.6; $p < 0.05$). The same results were obtained in H_2DCFDA-loaded PC3 cells (data not shown). These data suggest that **11** emulated other quinone inhibitors by irreversibly inhibiting Cdc25B through the production of ROS.[40,47,50]

We then tested the ability of the selected compounds to affect MCF-7 cell cycle by evaluating their effects on the G1/S and G2/M phase transitions; indeed, inhibitors of Cdc25 phosphatases affect cell proliferation by blocking the cell cycle progression. Asynchronously growing MCF-7 cells were exposed for different times to the chosen compounds at the above-reported concentration, and analyzed by flow cytometry, in order to determine the cell distribution among the different phases of the cell cycle (G0/G1, S, and G2/M). Control cells treated with DMSO alone proceeded through a normal cell cycle (Figure 11). After 24 h treatment, compounds **11** and **19** led to a statistically significant enrichment of G2/M cell population, as compared to the control (18.1% ± 0.03 and 26.6% ± 0.03 vs 9.4% ± 0.04, respectively), whereas compound **12** strongly decreased cells in S phase of cell cycle (3.3% ± 0.01 vs 9.35% ± 0.02). No significant effect was observed with compound **18** at 24 h. After 48 h treatment, MCF-7 cells showed a marked arrest in G0/G1 with a strong reduction of the cell population in the S phase of the cell cycle with all the tested compounds (2.6% ± 0.02, 3.2% ± 0.01, 1.8% ± 0.02, and 1.6% ± 0.01 vs 14.5% ± 0.02 for compounds **11**, **12**, **18**, and **19** vs control, respectively); the block at G1 phase persisted even after 72 h of incubation (data not shown).

Effects of Cdc25 Phosphatase Inhibitors on Cdk1 Phosphorylation Status. Inhibition of Cdc25 phosphatases should induce not only cell cycle arrest but also Cdk1 hyperphosphorylation.[7−12] Thus, we investigated the Cdk1 phosphorylation status in K562 cells treated with inhibitors **11**, **12**, **18**, and **19** for 24 h, with DMSO as a vehicle control. To this aim, cultures of K562 cells treated with the Cdc25 phosphatase inhibitors were analyzed by Western blotting using an antiphospho-Cdk1 (Y15) antibody or with an anti-Cdk1 antibody as a loading control (Figure 12). An increase in Cdk1 hyperphosphorylation was evident in cells treated with each inhibitor; on the other hand, cells treated with the DMSO vehicle showed no hyperphosphorylation of Cdk1 and likely continued to progress through the cell cycle. These results are consistent with what would be expected of an inhibitor of Cdc25B.

Refinement of Lead Cdc25B Inhibitor 19. Hierarchical screening is an efficient strategy allowing an initial broad search over a chemically and pharmacologically diverse set of compounds, followed by a focused search over a much larger database to find molecules related to potential lead compounds.[51] A similarity search over the full NCI database with the low-micromolar Cdc25B inhibitor **19** resulted in 34 compounds, which were docked to the Cdc25B crystal structure and ranked according to predicted Glide XP score. The top 19 compounds with the lowest scoring value for Cdc25B were selected for experimental testing (Table 3). Six of the 19 compounds showed >50% inhibition at 50 μM. In particular, compounds **34** [2-(4-(methylamino)-3-nitrobenzoyl)benzoic acid], **48** [3-(3,4-dioxo-3,4-dihydronaphthalen-1-ylamino)benzoic acid], and **49** [2-(3,4-dioxo-3,4-dihydronaphthalen-1-ylamino)-6-hydroxypyrimidine-4-carboxylic acid] strongly inhibited the Cdc25B activity with IC_{50} of 7.9, 4.2, and 9.9 μM, respectively (Table 3 and Supporting Information Figure S5). Irreversible inhibition of Cdc25B in vitro was seen when the enzyme was pretreated with compounds **48** and **49** up to 20 min, using a previously described dilution method[39] (Figure 13). These data suggest

dx.doi.org/10.1021/jm201624h | J. Med. Chem. 2012, 55, 4142−4158

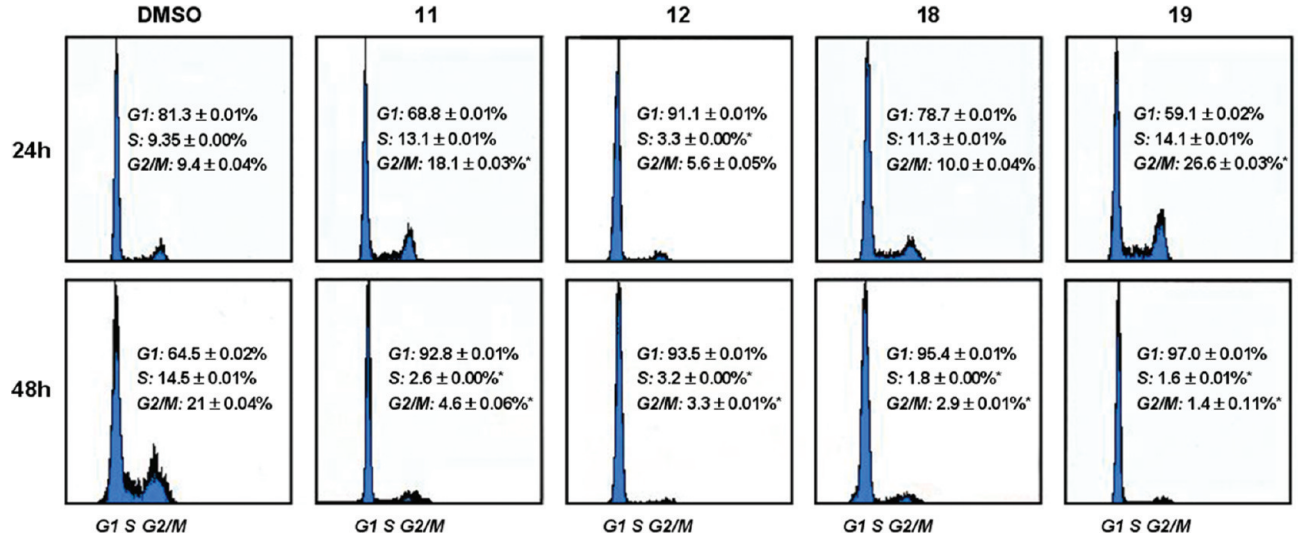

Figure 11. Cell cycle analysis of MCF-7 breast cancer cells treated with Cdc25B inhibitors **11** (20 μM), **12** (400 μM), **18** (400 μM), and **19** (200 μM). The values are the mean ± SD of three experiments. For details, see the Experimental Section.

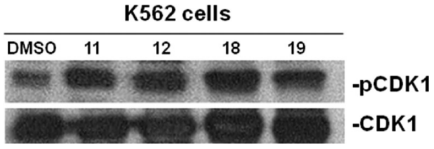

Figure 12. Cdk1 phoshorylation status after K562 cell treatment with Cdc25B inhibitors **11** (20 μM), **12** (400 μM), **18** (400 μM), and **19** (200 μM). After 24 h treatment, cells were lysed and analyzed by Western blotting. Cdk1 activity was evaluated using antiphospho-Cdk1 (Y15) antibody and detection of total Cdk1 served as a loading control.

that **48** and **49** behaved as other quinone inhibitors by irreversibly inhibiting Cdc25B. In contrast, the enzyme activity was almost completely restored in presence of compounds **34**, **39**, **43**, and **44**, so they were reversible inhibitors.

DISCUSSION AND CONCLUSION

Discovery of Cdc25 phosphatase inhibitors may be useful in targeted cancer therapies because of the oncogenic nature of Cdc25A and Cdc25B. Structurally diverse Cdc25 inhibitors have been discovered over the past few years, the most potent of which are quinone-based derivatives with IC_{50} values in the submicromolar range.[10,22,23] These compounds act mainly through irreversible linkage with the catalytic cysteine (C473 in Cdc25B) or vicinal serines[52] or oxidation and inactivation of the catalytic cysteine by ROS, either generated through in vitro redox cycling of these compounds in the presence of DTT or induced within cells by exposure to these compounds.[40,41,53]

In the attempt to identify potent and reversible inhibitors of Cdc25 phosphatases with new and original scaffolds, we carried out high-throughput virtual screenings on both NCI Diversity Set and ZINC databases targeting the active pocket of Cdc25B catalytic domain. The effect of the selected compounds was tested in vitro, either on cancer cell toxicity or as inhibition of the phosphatase activity of purified Cdc25B and Cdc25A.

Virtual screening led to the selection of 23 compounds from the NCI Diversity Set and seven compounds from the ZINC database. Fifteen among them were Cdc25 inhibitors on the basis of an in vitro assay for Cdc25A, -B and -C activity; however, the analysis was restricted to compounds representative of different types of inhibition, using a dilution method approach in the Cdc25 inhibition assay.[39] In particular, compound **11** [3-(4,5,6-trihydroxy-3-oxo-3*H*-xanthen-9-yl)-propanoic acid], a Cdc25B irreversible inhibitor, compound **12** [5-((2-hydroxy-4-methylquinolin-6-yl)methyl)-2-methoxy-benzenesulfonic acid], a Cdc25B reversible inhibitor, and compounds **18** [5,5′-(3-(pyridin-2-yl)-1,2,4-triazine-5,6-diyl)-difuran-2-sulfonic acid] and **19** [4-(2-carboxybenzoyl)phthalic acid], two Cdc25B inhibitors with intermediate behavior, were chosen for further studies.

Kinetic studies allowed a more detailed characterization of the mechanism of action of these molecules in terms of power and type of inhibition. Compound **11** exerted the highest inhibition power on purified catalytic domain of Cdc25B (IC_{50} = 0.10 μM; K_i = 0.08 μM). However, its kinetic behavior was compatible with that of an irreversible inhibitor of Cdc25B. Similar to several other quinone-based Cdc25 inhibitors,[40−42] compound **11** produced ROS in cells (Figure 10) and induced irreversible Cdc25B inhibition that was attenuated by a ROS-scavenger such as *Hp*SOD. These data support the hypothesis that redox cycling and production of ROS could be involved in the inhibition mechanism of Cdc25B by compound **11**.

On the contrary, compounds **12** and **18** were identified as reversible competitive inhibitors of Cdc25B, although their inhibition power was low (IC_{50} > 100 μM for both; K_i = 84 and 159 μM for **12** and **18**, respectively). Also, compound **19** was identified as a reversible competitive inhibitor of Cdc25B phosphatase activity, but its inhibition power (IC_{50} = 17.5 μM; K_i = 5.3 μM) made this molecule a promising lead compound for the development of new inhibitors for therapeutic potential. The specificity of the inhibitory effect was confirmed by the ability of the selected compounds to inhibit the phosphatase activity of Cdc25A, with a behavior similar to that observed for Cdc25B. Given the high sequence identity among Cdc25A and Cdc25B isoforms, especially in the active site region, it was not surprising to find the inhibitory effects in both Cdc25s. These data are relevant because, until recently, very few competitive and reversible inhibitors of Cdc25 dual specificity phosphatases have been discovered.

QikProp[54] from the Schrodinger Suite was run to estimate properties that are potentially important to compound

dx.doi.org/10.1021/jm201624h | *J. Med. Chem.* 2012, 55, 4142−4158

Table 3. Inhibition Properties of Analogues of Compound 19[a]

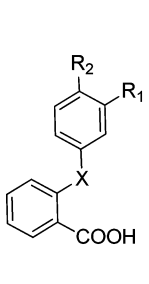

31-37

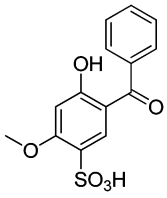

38

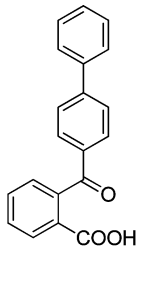

39

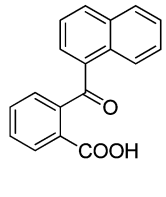

40

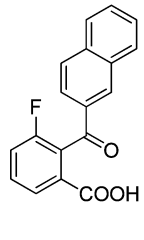

41

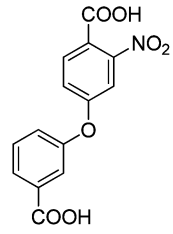

42

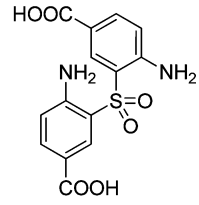

43

Cpd	NSC No.	R_1	R_2	X	Cdc25B Inhibition (%)	IC_{50} (μM)	QP log *P*	GLIDE XP Score
31	5003	H	COOH	CO	12	-	1.959	-6.94
32	15368	NO_2	OH	CO	13	-	1.102	-6.33
33	15366	NO_2	Cl	CO	13	-	0.340	-6.12
34	156744	NO_2	$NHCH_3$	CO	65	7.9	1.613	-6.42
35	55778	NO_2	H	CO	17	-	1.652	-6.33
36	74563	H	$COCH_3$	CO	20	-	2.262	-6.11
37	113996	COOH	H	NH	18	-	2.666	-7.26
38	60584				49	-	1.559	-5.83
39	75270				54	23.1	3.892	-6.19
40	59936				41	-	3.269	-5.78
41	171259				34	-	3.516	-6.48
42	59761				37	-	1.652	-7.10
43	238165				62	20.1	0.319	-6.26

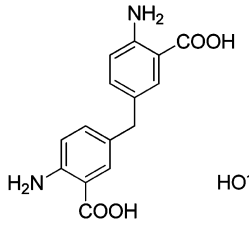

44

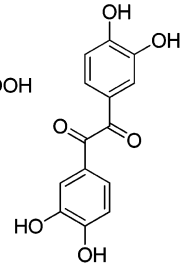

45

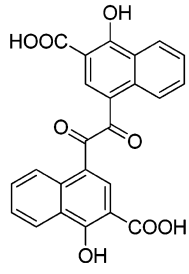

46

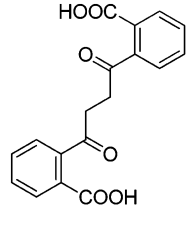

47

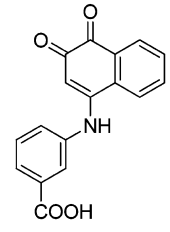

48

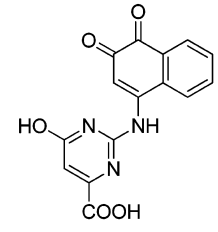

49

44	37136				52	23.8	0.940	-7.14
45	42520				22	-	-0.272	-7.02
46	292213				26	-	2.257	-6.40
47	518963				20	-	0.692	-7.04
48	117023				85	4.2	1.458	-7.77
49	125252				60	9.9	-0.046	-7.67

[a]Percent of inhibition of Cdc25B phosphatase activity was measured at 50 μM concentration of the inhibitor; values of experimental IC_{50} for inhibition of Cdc25B and predicted GLIDE XP score were obtained as described in the Experimental Section.

solubility, permeability, and drug development. As depicted in Table 2, almost all the calculated properties of **11**, **12**, **18**, and **19** were in the ranges predicted by QikProp for 95% of known oral drugs, a finding indicating the potential for further optimizations as drug leads. However, permeability across biological membranes was limited due to their highly charged carboxylate or sulfonate moieties. The predicted apparent Caco-2 cell permeability value (QP P_{Caco}, an additional parameter of permeability that is used as a model for the gut−blood barrier)[55] was <25 nm/s for **11**, **18**, and **19** (suggesting poor permeability) and 25−500 nm/s for **12** (suggesting moderate permeability). Compound **19** has no predicted primary metabolites, but compounds **11**, **12**, and **18** have a number of primary metabolites in the allowed range (1/8).

Regarding the effect of compounds **11**, **12**, **18**, and **19** on cell cycle, all tested compounds significantly inhibited MCF-7, PC-3, and K562 cell proliferation, even in the presence of serum; other reversible Cdc25 inhibitors, such as indolylhydroxyquinones, although more potent, were ineffective in cellular assays due to a specific binding to bovine serum albumin.[39]

Furthermore, all selected compounds significantly affected MCF-7 breast cancer cell cycle progression. This is relevant because a recently identified competitive reversible Cdc25

dx.doi.org/10.1021/jm201624h | J. Med. Chem. 2012, 55, 4142−4158

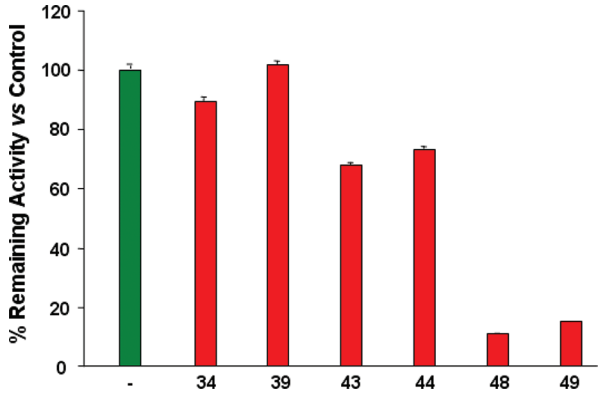

Figure 13. Reversibility of Cdc25B inhibition by analogues of the low-micromolar inhibitor **19**. Cdc25B (0.5 μg) was incubated for 20 min at room temperature with 50 μM of the indicated inhibitors or DMSO as a vehicle control. Following a 10-fold dilution, the residual activity was measured as reported in the Experimental Section upon addition of OMFP. Results are expressed as a percent of residual activity (red bars) vs untreated control (green bar) and represent the averages ± SD of three different determinations.

inhibitor, 5169131, was unable to affect cell cycle progression in asynchronous cells.[50] Indeed, our results indicated that, after 24 h of incubation, compounds **11** and **19** led to a statistically significant enrichment of G2/M cell population. After 48 h treatment, all selected compounds determined a marked arrest in G0/G1 with a strong reduction of the cell population in the S phase of the cell cycle; the block at G0/G1 phase persisted even after 72 h of incubation. Therefore, we can hypothesize that compounds **11** and **19** regulate cell cycle progression by first exerting their effect on Cdc25B, thus inducing a G2/M phase arrest, and then acting on Cdc25A and causing a G0/G1 arrest. These compounds could behave as caulibugulone A, a selective in vitro inhibitor of Cdc25 phosphatases; it arrested cells in G1 and G2/M phases of the cell cycle by inhibiting both Cdc25B and Cdc25A activity.[49] Unlike compound **11** and **19**, compounds **12** and **18** only caused a G0/G1 arrest in MCF-7 cells, whereas they did not seem to exert any effect on G2/M phase of cell cycle, so they could preferentially act on Cdc25A, even though they have been selected against Cdc25B. This hypothesis was confirmed by the lower inhibition properties exerted by these compounds on Cdc25B activity with respect to **11** and **19**. The cell cycle arrest was also accompanied by increased phosphorylation of Cdk1, a substrate of Cdc25; this behavior indicates the specificity of these compounds toward the Cdc25s. In addition to identifying new inhibitors by virtual docking, we also modeled the interactions between the identified inhibitors and the catalytic domain of both Cdc25A and Cdc25B (Figure 8 and Figure S4 of Supporting Information), thus providing a structural rationale for the in vitro observations.

A secondary screening, coupled with structural similarity searching of the low-micromolar lead **19**, resulted in the additional set of 19 ligands, and six among them (**34**, **39**, **43**, **44**, **48**, and **49**) were inhibitors of Cdc25B. In particular, compounds **34**, **48**, and **49** had promising IC_{50} values of 7.9, 4.2, and 9.9 μM, respectively. The docked conformations of the secondary screening hits matched that of the lead inhibitor **19**. This approach resembles the so-called hierarchical filtering. In our case, the first pass was used to discover the appropriate scaffolds through focusing on compound structural diversity. At this stage, utilization or construction of a structurally diverse library is the key. The second pass was to uncover the best analogues of the compounds discovered in the first pass.

Here, we have identified a number of small molecules that inhibit Cdc25B phosphatase and also inhibit the proliferation of human cancer cells, such as MCF-7, PC-3, and K562. The combination of computational, biochemical, and cell biology experiments allowed the identification of a variety of structurally distinct inhibitors for a phosphatase target without the need for a massive high-throughput chemical screen. Thus, collaboration between biochemical and virtual screening provides an extraordinarily effective approach to drug discovery. Further refinement of these compounds, to tune them to higher affinity and more specific inhibition, offers a great therapeutic potential, given the strategic position of Cdc25 in cell survival pathways.

EXPERIMENTAL SECTION

Protein Structure Template Preparation. Among the ligand-free Cdc25B crystal structures present in the PDB database,[56] the best candidates for a docking study are 1CWT (resolution 2.3 Å),[20] 1QB0 (resolution 1.91 Å),[20] and 1YMK (apo form, resolution 1.7 Å).[57] In addition, one Cdc25B structure cocrystallized with a modified peptide that blocks the active site has been reported in a recent patent application by BASF.[58] Overlay of 1CWT, 1QB0, BASF, and 1YMK structures showed that almost all of them share a highly similar binding site conformation. The most significant difference observed among the experimental structures resides in the conformation of R544 side chain: in 1CWT, 1QB0, and 1YMK, it occludes the swimming pocket, whereas in BASF structure, the peptide ligand pushes it away, opening the pocket. Therefore, docking experiments were carried out employing the crystal structure of 1QB0, in which the side chain conformation of R544 was manually oriented as in the BASF structure. All crystallographic water molecules and other chemical components were omitted, the right bond orders as well as charges and atom types were assigned, and hydrogen atoms were added to the crystal structure using Maestro.[59] Arg, Lys, Glu, and Asp residues were considered ionized, while His was considered as neutral. Then the protein was submitted to a series of restrained, partial minimizations using the OPLS-AA force field[60] within the "Protein and Ligand Preparation" module of GLIDE version 5.7.[35] To compensate for the fixed protein structure, which is not expected to be optimal for a particular ligand, the van der Waals radii for nonpolar ligand atoms were scaled by a factor of 0.8, thereby decreasing penalties for close contacts. Receptor atoms were not scaled.

Library of Chemical Compounds. Drug-like subset of ZINC database[34] and NCI Diversity Set (http://dtp.nci.nih.gov/branches/dscb/repo_open.html) were selected for the virtual screening study. The NCI Diversity Set was preprocessed with the GLIDE module "LigPrep", which prepared the ligands in multiple protonation and tautomerization states. This procedure resulted in ~2392 structures as compared to the initial 1990 of the NCI Diversity Set. The ZINC "drug-like" set (subset no. 3, as defined in ZINC version 7) had already been preprocessed and includes multiple protonation and tautomerization states.[34] The complete virtual library, prefiltered for properties based on Lipinski's rules,[61] totaled about 2.1 million compounds.

Ligand Docking and Compound Selection Procedures. Virtual screening and docking were performed using GLIDE with default docking parameter settings. The grid-enclosing box, which must contain the center of each ligand docked, was centered on the sulfur atom of C473 and defined to enclose residues located within 14 Å from the catalytic thiolate, while the outer box, in which all parts of the ligand must bind, was 31 Å in each direction. A van der Waals radius scaling factor of 0.80 for atoms with a partial atomic charge (absolute value) less than 0.15 was used in order to soften the potential for nonpolar parts of the receptor. Next, a "funnel" strategy was employed for virtual screening. For the large ZINC library, GLIDE was run in the high-throughput virtual screening (HTVS) mode to

dx.doi.org/10.1021/jm201624h | J. Med. Chem. 2012, 55, 4142–4158

perform a complete conformational and positional search of three-dimensional space in the active site. For the compounds that scored in the highest 2% (40000), GLIDE SP (standard precision)[62] was run. Similarly for the top 20% high scoring GLIDE SP compounds (8000), GLIDE XP (extra precision)[63] was run too. The 80 top-ranked structures (1%) were kept for successive analysis. For the small NCI diversity set library, the HTVS step was skipped and the compounds were docked in GLIDE SP and XP modes, keeping, respectively, 410 (20%) and 128 (30%) top-ranked structures. In essence, GLIDE performs a thorough conformational search for a ligand; then it determines all reasonable orientations ("poses") for each low-energy conformer in the designated binding site. In the process, torsional degrees of the ligand are relaxed, although the protein conformation is fixed. The SP "scoring function" is applied to judge the poses by considering, for example, hydrophobic and electrostatic interactions, hydrogen bonding, steric clashes, desolvation and internal energy of the ligand, and possible trapped or bridging water molecules in the binding site. In XP mode, the poses are further relaxed by complete energy minimizations. The resultant more accurate structures provide a basis for more detailed evaluation of contributions from explicit water molecules in the binding site and hydrophobic interactions.

The homology-modeled structure of Cdc25A[46] was used as the receptor model for docking simulations of compounds **11** and **18**. Side chain conformations of R436 and R439 of Cdc25A were manually oriented as those of R479 and R482 in the 1QB0 structure of Cdc25B, while the side-chain conformation of R501 was manually oriented as that of R544 in the BASF structure of Cdc25B.

DFT Calculations. Geometry optimizations of both **11a** and **11b** tautomers were performed using the Jaguar 7.8 suite of ab initio quantum chemistry programs[64] at the B3LYP/6-31G* level of theory.[65] The coupling of DFT with a Poison−Boltzmann (PB) continuum solvent can provide accurate estimates of the solvation free energies of the two tautomers in water.[66] This involves the numerical solution of the PB equation to determine the self-consistent reaction field (SCRF) of the solvent acting on the quantum mechanical solute. In this approach, the solute is described as a low-dielectric cavity (ε_{solute} = 1.0) immersed in a continuum solvent characterized by two properties: the solvent probe radius (r_{probe} = 1.4 for water) and the solvent dielectric constant ($\varepsilon_{solvent}$ = 80.0) for water. The dielectric solute/solvent boundary was taken as the solvent-accessible surface area (SASA) defined by the probe radius. The charge distribution of the solute was represented by atom-centered point charges based on electrostatic potential (ESP) fits. The nonelectrostatic component (e.g., cavity term) of the solvation free energy was calculated using the empirical relation given in ref 67. The atomic radii used to determine the van der Waals envelope of the solute were taken from Tannor et al.[67] without modifications[68] (1.9 Å for sp^3-hybridized carbon, 1.6 Å for oxygen, and 1.15 Å for hydrogen). Calculations were carried out using both gas-phase geometries and geometries optimized in the solvent reaction field.

Hierarchical Similarity Search. An online search utility provided by the NCI (http://129.43.27.140/ncidb2/)[69] was used to search the entire NCI database for compounds similar to Cdc25B inhibitor **19**. Two methods were used to judge compound similarity: search on the basis of substructure by SMILES string (http://daylight.com) and/or similarity by Tanimoto coefficient,[70] with a cutoff of 0.85.[71] From these searches, selected compound structures were docked to Cdc25B crystal structure and ranked according to predicted GLIDE XP score. Compounds with the lowest scoring value were requested and assayed for effect on phosphatase activity as described above.

Materials and Reagents. All compounds were purchased from commercial vendors or kindly provided by the National Cancer Institute (http://dtp.cancer.gov). The identity and purity of the assayed compounds was independently assessed by elemental analysis and ^{1}H NMR (see Supporting Information). Compounds were dissolved in DMSO, and stock solutions at 10 mM concentration were prepared. OMFP was from Sigma. The recombinant forms of Cdc25A and Cdc25B catalytic domain were purified essentially as previously described,[72] using a heterologous expression system constituted by the vectors pET28a-CDC25A-cd and pET28a-CDC25B-cd, kindly provided by H. Bhattacharjee (Florida International University, Herbert Wertheim College of Medicine, Miami, Florida), and the *Escherichia coli* BL21(DE3) strain from Novagen. The purified samples of recombinant Cdc25A and Cdc25B were homogeneous when analyzed by SDS polyacrylamide gel electrophoresis or RP-HPLC on a C4 column. Furthermore, the analysis by ESI-Q/TOF MS gave molecular masses of 22833.37 ± 0.08 and 22841.81 ± 0.09 Da for Cdc25A and Cdc25B, respectively, almost coincident with those predicted by the amino acid sequences, including the N-terminal His-tag and excluding the initial methionine. All other reagents were of analytical grade.

In Vitro Enzyme Assays. Phosphatase activity of Cdc25A, -B, and -C was measured through a fluorimetric method, using OMFP as a synthetic substrate; following its hydrolysis, *O*-methylfluorescein product was formed and detected by a fluorescence measurement. In the initial screening experiments, a commercially available Protein Phosphatase Cdc25 Fluorimetric Assay kit (Cyclex Co, Nagano, Japan) and a 96-well microtiter plate fluorescence reader (Becton Dickinson 353948, New Jersey, USA) were employed. Mixtures, prepared according to manufacturer's instruction, contained OMFP and 100 μM of each inhibitor; the reaction started by the addition of Cdc25A, -B, or -C, and the fluorescence emission was measured after 15 min at room temperature, setting excitation and emission filters of the reader at 485 and 538 nm, respectively. Vanadate was used as a positive control of inhibition; in the absence of inhibitor, DMSO was used as a vehicle control. It should be emphasized that the tested inhibitors at micromolar concentrations are not fluorescent and do not exhibit a detectable absorbance at the excitation wavelength used in the in vitro assays. Moreover, neither Cdc25B nor Cdc25A displays a detectable fluorescence/absorbance in our experimental conditions.

The above cited kit was also employed for studying the reversibility of Cdc25B inhibition through a protocol similar to the dilution method previously described.[39] Cdc25B was incubated for 20 min at room temperature with 100 μM of each inhibitor or DMSO as vehicle control. Samples were then 10-fold diluted, and the remaining phosphatase activity was determined as reported above. The residual enzyme activity was referred to that measured with vehicle alone.

For steady-state enzyme kinetic studies, the phosphatase activity of purified recombinant Cdc25A or Cdc25B was measured at 30 °C using a computer-assisted Cary Eclipse spectrofluorimeter (Varian) equipped with an electronic temperature controller. Excitation and emission wavelength was set at 485 and 530 nm, respectively; excitation and emission slits were both set at 20 nm for Cdc25A and 10 nm for Cdc25B. The reaction mixture contained 50 nM Cdc25A or 10 nM Cdc25B and appropriate concentrations of inhibitor in 500 μL final volume of 20 mM Tris-HCl, pH 7.8, 1 mM DTT. DMSO was used as a vehicle control. The reaction started by the addition of 1−25 μM OMFP, and fluorescence was monitored continuously. The rate of OMFP hydrolysis was measured in the linear part of the fluorescence increase and expressed as arbitrary units (AU) per min. Blanks run in the absence of enzymes and/or inhibitor were subtracted. The concentration of inhibitor leading to 50% inhibition (IC_{50}) was obtained from profiles of residual phosphatase activity realized in the presence of 25 μM OMFP and different inhibitor concentrations. The data were then linearized in semilogarithm plots for the evaluation of the IC_{50} from the slope of the equation. Linear curve fits were obtained with the least-squares method, and the significance of the correlation was estimated from the squared correlation coefficient r^2, which was always higher than 0.95. The K_m for OMFP and the maximum rate of OMFP hydrolysis ($\Delta AU/min_{max}$) were obtained from Lineweaver−Burk plots, carried out in the absence or in the presence of different inhibitor concentrations. For the calculation of the inhibition constant (K_i), the equation used depended on the type of inhibition. In the reversible competitive inhibition, K_i was averaged from the increase of K_m for OMFP in the presence of the inhibitor, according to $K_m' = K_m\{1 + ([I]/K_i)\}$, where K_m' represents the K_m for OMFP measured in the presence of the concentration [I] of the inhibitor. In the irreversible inhibition, K_i was averaged from the decrease of $\Delta AU/min_{max}$ in the presence of the inhibitor, according to $\Delta AU/min_{max}' = \Delta AU/min_{max}/\{1 + ([I]/K_i)\}$, where $\Delta AU/min_{max}'$

dx.doi.org/10.1021/jm201624h | J. Med. Chem. 2012, 55, 4142−4158

represents the maximum rate of OMFP hydrolysis measured in the presence of the concentration [I] of the inhibitor.

Cell Cultures. Human MCF-7 breast and human PC-3 prostate cancer cells were cultured in DMEM, while human acute myeloid leukemia K562 cells in RPMI, supplemented with 5% fetal bovine serum (FBS) (Life Technologies, Gaithersburg, MD, USA) and 2-mM L-glutamine at 37 °C under a 5% CO_2 atmosphere. Each cell line was grown in 100 mm culture dishes (BD Falcon, New Jersey, USA) and used for biological assays.

Antiproliferative Assays. Antiproliferative effects of the selected compounds were determined by MTS (3-(4,5-dimethylthiazole-2yl)-5-(3-carboxymethoxyphenyl)-2-(4-sulfophenyl)-2*H*-tetrazolium, inner salt) and PES (phenazine ethosulfate) assay (CellTiter 96 AQ_{ueous} One Solution Reagent) provided by Promega (Madison, WI, USA).[73] In brief, cells were plated at 5000 cells per well in 96-well microtiter plates (BD Falcon 353072, New Jersey, USA) with 100 μL DMEM growth medium containing 5% FBS; 24 h after seeding, cells were treated with different concentrations of the selected compounds or DMSO as a vehicle control for 24, 48, or 72 h. Then, 20 μL/well of CellTiter 96 AQ_{ueous} One Solution Reagent was added and, after incubation at 37 °C for 4 h, the absorbance was determined by an ELISA reader (Bio-Rad, Hercules, California, USA) at a wavelength of 490 nm.

Cell Cycle Analysis. Log phase cells were seeded out using DMEM 5% FBS at $1 \times 10^6 \times 100$ mm culture dish, and the cells were allowed to attach for 24 h at 37 °C. The compounds were added to the cells and incubated for additional 24, 48, or 72 h. After incubation, the cells were harvested with trypsin and fixed with cold 70% ethanol. Cells were then treated with 100 μg/mL RNase-DNase free, stained with 5 μg/μL propidium iodide, and analyzed for cell cycle status profile using a FACScan flow cytometer (Becton Dickinson, USA).

Measurement of Cellular ROS Generation. ROS were detected using 2′,7′-dichlorodihydrofluorescein diacetate (H_2DCFDA; Calbiochem, Milan, Italy). H_2DCFDA diffuses into the cells, where it is converted into a nonfluorescent derivative (H_2DCF) by endogenous esterases. H_2DCF is oxidized to green fluorescent 2′,7′-dichlorofluorescein (DCF) in the presence of intracellular ROS. Briefly, K562 cells (1×10^6) were harvested by centrifugation, washed, resuspended in phosphate-buffered saline (PBS) alone or in the presence of 1 mM DTT, and incubated for 30 min at 37 °C, 5% CO_2. Cells were further incubated with 10 μM H_2DCFDA for 30 min, washed, resuspended in PBS, and then treated with DMSO (vehicle control) or with compound **11** for 30 min at 37 °C, 5% CO_2. After an additional wash, DCF fluorescence was measured by flow cytometry using the FACSCalibur flow cytometer (BD Pharmingen). About 30000 events (i.e., fluorescence readings corresponding to no less than 20000 cells) were recorded for each sample.[74]

Western Blotting and Antibodies. K562 cells were plated at 5×10^5 cells per well in 6-well plates (BD Falcon 353046, New Jersey, USA) in RPMI growth medium containing 5% FBS; 24 h after seeding, cells were treated with different concentrations of the selected compounds or DMSO, as a vehicle control, for 24 h. Cells were harvested by centrifugation, lysed in lysis buffer (50 mM Tris HCl, pH7.5, 250 mM NaCl, 0.1%Triton X-100, 5 mM EDTA, 50 mM NaF) supplemented with protease and phosphatase inhibitors cocktail (Sigma, St. Louis, MO), for 30 min on ice followed by centrifugation at 12000*g* for 15 min. Cleared lysates were assayed for protein concentration by a colorimetric assay (Bio-Rad, Hercules, CA). Then 50 μg of protein was loaded on a 12% SDS-PAGE and transferred on a PVDF membrane. The membrane was blocked with 5% nonfat dry milk and probed with 1:1000 anti-phoshoY15-Cdk1 (9111; Cell Signaling, Danvers, MA) and 1:1000 anti-cdc2p34(17) (sc-54; Santa Cruz Biotechnology, CA), the latter used as a loading control. Bound primary antibodies were detected with either horseradish peroxidase–goat antirabbit antibody or horseradish peroxidase–goat antimouse antibody (Bio-Rad). Immunoreactive bands were detected by ECL according to the manufacturer's instructions (Amersham, Little Chalfont, UK).

■ ASSOCIATED CONTENT

Supporting Information

Dose-dependent inhibition profile of Cdc25A by compounds **11**, **12**, **18**, and **19**; SDS/PAGE of Cdc25B samples treated with inhibitor **11**; dose-dependent effect of inhibitor **11** on Cdc25B; binding modes of compounds **11** and **19** into the Cdc25A binding cavity as calculated by GLIDE; concentration–response plots of analogue inhibitors **34**, **39**, **43**, **44**, **48**, and **49**; elemental analysis and ^{1}H NMR data of the active inhibitors **11**, **12**, **18**, **19**, **34**, **39**, **43**, **48**, and **49** (PDF). Results of in silico screen for the 128 top-ranked structures from NCI Diversity Set and the 80 top-ranked ones from the ZINC database (XLS). This material is available free of charge via the Internet at http://pubs.acs.org.

■ AUTHOR INFORMATION

Corresponding Author

*Phone: +39-081-678613. Fax: +39-081-678012. E-mail: lavecchi@unina.it.

Notes

The authors declare no competing financial interest.

■ ACKNOWLEDGMENTS

Gratitude is expressed to the National Cancer Institute for providing test compounds free of charge. We also thank Dr. Hiranmoy Bhattacharjee for the gift of the vectors expressing Cdc25B and Cdc25A. We also thank Dr. Hwangseo Park for providing us with the coordinates of the homology-modeled structure of Cdc25A. HPLC and mass spectrometry analysis were due to the courtesy of Drs. Angela Chambery and Antimo Di Maro, Second University of Naples. This work was financially supported by MIUR (PRIN 2008, prot. 200879X9N9 to A.L. and PRIN 2009, prot. 2009P2HZZ7 to E.D.V. and M.M.), Rome, Italy.

■ ABBREVIATIONS USED

Cdc25, cell division cycle 25; Cdk, cyclin-dependent kinases; DFT, density functional theory; DMEM, Dulbecco's Modified Eagle's Medium; DMSO, dimethyl sulfoxide; DSP, dual-specificity phosphatase; DTT, dithiothreitol; ES, phenazine ethosulfate; ESI-Q/TOF MS, electrospray ionization quadrupole time-of-flight mass spectrometry; FBS, fetal bovine serum; H_2DCFDA, 2′,7′-dichlorodihydrofluorescein diacetate; H_2DCF, 2′,7′-dichlorodihydrofluorescein; DCF, 2′,7′-dichlorofluorescein; *Hp*SOD, Superoxide dismutase from *Helicobacter pylori*; HTVS, high-throughput virtual screening; K562, human chronic myelogenous leukemia cells; MCF-7, human breast cancer cells; MTS, 3-(4,5-dimethylthiazole-2yl)-5-(3-carboxymethoxyphenyl)-2-(4-sulfophenyl)-2*H*-tetrazolium, inner salt; NCI, National Cancer Institute; OMFP, 3-*O*-methyl fluorescein phosphate; PBS, phosphate-buffered saline; PC-3, prostate cancer cells; PDB, Protein Data Bank; PTP, protein tyrosine phosphatase; ROS, reactive oxygen species; RP-HPLC, reversed-phase high-performance liquid chromatography; SDS/PAGE, sodium dodecyl sulfate polyacrylamide gel electrophoresis

■ REFERENCES

(1) Nilsson, I.; Hoffman, I. Cell cycle regulation by the Cdc25 phosphatase family. *Prog. Cell Cycle Res.* **2000**, *4*, 107–144.

(2) Jinno, S.; Suto, K.; Nagata, A.; Igarashi, M.; Kanaoka, Y.; Nojima, H.; Okayama, H. Cdc25A is a novel phosphatase functioning early in the cell cycle. *EMBO J.* **1994**, *13*, 549−556.
(3) Forrest, A. R.; McCormack, A. K.; DeSouza, C. P.; Sinnamon, J. M.; Tonks, I. D.; Hayward, N. K.; Ellem, K. A.; Gabrielli, B. Multiple splicing variants of Cdc25B regulate G_2/M progression. *Biochem. Biophys. Res. Commun.* **1999**, *260*, 510−515.
(4) Donazelli, M.; Draetta, G. F. Regulating mammalian checkpoints through Cdc25 inactivation. *EMBO J.* **2003**, *4*, 671−677.
(5) Molinari, M.; Mercurio, C.; Dominguez, J.; Goubin, F.; Draetta, G. F. Human Cdc25A inactivation in response to S phase inhibition and its role in preventing premature mitosis. *EMBO Rep.* **2000**, *1*, 71−79.
(6) Mailand, N.; Falck, J.; Lukas, C.; Syljuasen, R. G.; Welcker, M.; Bartek, J.; Lukas, J. Rapid destruction of human Cdc25A in response to DNA damage. *Science* **2000**, *288*, 1425−1429.
(7) Santamaria, D.; Barriere, C.; Cerqueira, A.; Hunt, S.; Tardy, C.; Newton, K.; Caceres, J. F.; Dubus, P.; Malumbres, M.; Barbacid, M. Cdk1 is sufficient to drive the mammalian cell cycle. *Nature* **2007**, *448*, 811−816.
(8) Boutros, R.; Dozier, C.; Ducommun, B. The when and wheres of Cdc25 phosphatases. *Curr. Opin. Cell Biol.* **2006**, *18*, 185−191.
(9) Boutros, R.; Lobjois, V.; Ducommun, B. CDC25 phosphatases in cancer cells: key players? Good targets? *Nature Rev. Cancer* **2007**, *7*, 495−507.
(10) Lavecchia, A.; Di Giovanni, C.; Novellino, E. Cdc25A and B Dual-Specificity Phosphatase Inhibitors: Potential Agents for Cancer Therapy. *Curr. Med. Chem.* **2009**, *16*, 1831−1849.
(11) Rudolph, J. Cdc25 phosphatases: structure, specificity, and mechanism. *Biochemistry* **2007**, *46*, 3595−3604.
(12) Galaktionov, K.; Lee, A. K.; Eckstein, J.; Draetta, G.; Meckler, J.; Loda, M.; Beach, D. Cdc25 phosphatases as potential human oncogenes. *Science* **1995**, *269*, 1575−1577.
(13) (a) Hernàndez, S.; Bessa, X.; Beà, S.; Hernàndez, L.; Nadal, A.; Mallofré, C.; Muntane, J.; Castells, A.; Fernàndez, P. L.; Cardesa, A.; Campo, E. Differential expression of Cdc25 cell-cycle-activating phosphatases in human colorectal carcinoma. *Lab. Invest.* **2001**, *81*, 465−473. (b) Takemara, I.; Yamamoto, H.; Sekimoto, M.; Ohue, M.; Noura, S.; Miyake, Y.; Matsumoto, T.; Aihara, T.; Tomita, N.; Tamaki, Y.; Sakita, I.; Kikkawa, N.; Matsuura, N.; Shiozaki, H.; Monden, M. Overexpression of Cdc25B phosphatase as a novel marker of poor prognosis of human colorectal carcinoma. *Cancer Res.* **2000**, *60*, 3043−3050.
(14) Hernàndez, S.; Hernandez, L.; Bea, S.; Pinyol, M.; Nayach, I.; Bellosillo, B.; Nadal, A.; Ferrer, A.; Fernandez, P. L.; Montserrat, E.; Cardesa, A.; Cardes, E.; Campo, E. Cdc25A and the splicing variant Cdc25B2, but not Cdc25B1, -B3 or -C, are overexpressed in aggressive human non-Hodgkin's lymphomas. *Int. J. Cancer* **2000**, *89*, 148−152.
(15) Ngan, E. S. W.; Hashimoto, Y.; Ma, Z.-Q.; Tsai, M. J.; Tsai, S. Y. Overexpression of Cdc25B, an androgen receptor coactivator, in prostate cancer. *Oncogene* **2003**, *22*, 734−739.
(16) Guo, J.; Kleeff, J.; Li, J.; Ding, J.; Hammer, J.; Zhao, Y.; Giese, T.; Korc, M.; Büchler, M. W.; Friess, H. Expression and functional significance of Cdc25B in human pancreatic ductal adenocarcinoma. *Oncogene* **2004**, *23*, 71−81.
(17) (a) Wu, W. G.; Fan, Y. H.; Kemp, B. L.; Walsh, G.; Mao, L. Overexpression of Cdc25A and Cdc25B is frequent in primary nonsmall cell lung cancer but is not associated with overexpression of c-myc. *Cancer Res.* **1998**, *58*, 4082−4085. (b) Sasaki, H.; Yukiue, H.; Kobayashi, Y.; Tanahashi, M.; Moriyama, S.; Nakashima, Y.; Fukai, I.; Kiriyama, M.; Yamakawa, Y.; Fujii, Y. Expression of the Cdc25B gene as a prognosis marker in non-small cell lung cancer. *Cancer Lett.* **2001**, *173*, 187−192.
(18) Fernandez-Vidal, A.; Ysebaert, L.; Didier, C.; Betous, R.; Toni, F. D.; Prade-Houdellier, N.; Demur, C.; Contour-Galcera, M.-O.; Prevost, G. P.; Ducommun, B.; Payrastre, B.; Racaud-Sultan, C.; Manenti, S. Cell adhesion regulates Cdc25A expression and proliferation in acute myeloid leukemia. *Cancer Res.* **2006**, *66*, 7128−7135.
(19) Fauman, E. B.; Cogswell, J. P.; Lovejoy, B.; Rocque, W. J.; Holmes, W.; Montana, V. G.; Piwnica-Worms, H.; Rink, M. J.; Saper, M. A. Crystal structure of the catalytic domain of the human cell cycle control phosphatase, Cdc25A. *Cell* **1998**, *93*, 617−625.
(20) Reynolds, R. A.; Yem, A. W.; Wolfe, C. L.; Deibel, M. R.; Chidester, C. G.; Watenpaugh, K. D. Crystal structure of the catalytic subunit of Cdc25B required for G2/M phase transition of the cell cycle. *J. Mol. Biol.* **1999**, *293*, 559−568.
(21) Rudolph, J. Targeting the Neighbor's Pool. *Mol. Pharmacol.* **2004**, *66*, 780−2.
(22) Lavecchia, A.; Coluccia, A.; Di Giovanni, C.; Novellino, E. Cdc25B phosphatase inhibitors in cancer therapy: latest developments, trends and medicinal chemistry perspective. *Anticancer Agents Med. Chem.* **2008**, *8*, 843−856.
(23) Lavecchia, A.; Di Giovanni, C.; Novellino, E. Inhibitors of Cdc25 Phosphatases as Anticancer Agents—A Patent Review. *Expert Opin. Ther. Pat.* **2010**, *20*, 405−425.
(24) (a) Nishikawa, Y.; Carr, B. I.; Wang, M.; Kar, S.; Finn, F.; Dowd, P.; Zheng, Z. B.; Kerns, J.; Naganathan, S. Growth inhibition of hepatoma cells induced by Vitamin K and its analogs. *J. Biol. Chem.* **1995**, *270*, 28304−28310. (b) Tamura, K.; Southwick, E. C.; Kerns, J.; Rosi, K.; Carr, B. I.; Wilcox, C.; Lazo, J. S. *Cancer Res.* **2000**, *60*, 1317−1325.
(25) Lazo, J. S.; Nemoto, K.; Pestell, K. E.; Cooley, K.; Southwick, E. C.; Mitchell, D. A.; Furey, W.; Gussio, R.; Zaharevitz, D. W.; Joo, B.; Wipf, P. Identification of a potent and selective pharmacophore for Cdc25 dual specificity phosphatase inhibitors. *Mol. Pharmacol.* **2002**, *61*, 720−728.
(26) Cao, S.; Forster, C.; Brisson, M.; Lazo, J. S.; Kingston, D. G. I. Halenaquinone and xestoquinone derivatives, inhibitors of Cdc25B phosphatase from a *Xestospongia* sp. *Bioorg. Med. Chem.* **2005**, *13*, 999−1003.
(27) (a) Brezak, M. C.; Quaranta, M.; Contour-Galcera, M. O.; Lavergne, O.; Mondesert, O.; Auvray, P.; Kasprzyk, P. G.; Prevost, G.; Ducommun, B. Inhibition of human tumor cell growth in vivo by an orally bioavailable inhibitor of CDC25 phosphatases. *Mol. Cancer Ther.* **2005**, *4*, 1378−1387. (b) Cazales, M.; Boutros, R.; Brezak, M. C.; Chaumeron, S.; Prévost, G.; Ducommun, B. Pharmacologic inhibition of CDC25 phosphatases impairs interphase microtubule dynamics and mitotic spindle assembly. *Mol. Cancer Ther.* **2007**, *6*, 318−325.
(28) Brezak, M. C.; Valette, A.; Quaranta, M.; Galcera-Contour, M. O.; Jullien, D.; Lavergne, O.; Frongia, C.; Bigg, D.; Kasprzyk, P. G.; Prevost, G.; Ducommun, B. IRC-083864, a novel bis quinone inhibitor of CDC25 phosphatases active against human cancer cells. *Int. J. Cancer* **2009**, *124*, 1449−1456.
(29) Lavecchia, A.; Cosconati, S.; Limongelli, V.; Novellino, E. Modeling of Cdc25B dual specificity protein phosphatase inhibitors: docking of ligands and enzymatic inhibition mechanism. *ChemMedChem* **2006**, *1*, 540−550.
(30) Park, H.; Bahn, Y. J.; Jung, S.-K.; Jeong, D. G.; Lee, S.-H.; Seo, I.; Yoon, T.-S.; Kim, S. J.; Ryu, S. E. Discovery of novel Cdc25 phosphatase inhibitors with micromolar activity based on the structure-based virtual screening. *J. Med. Chem.* **2008**, *51*, 5533.
(31) Thor, H.; Smith, M. T.; Hartzell, P.; Bellomo, G.; Jewell, S. A.; Orrenius, S. The metabolism of menadione (2-methyl-1,4-naphthoquinone) by isolated hepatocytes. A study of the implications of oxidative stress in intact cells. *J. Biol. Chem.* **1982**, *257*, 12419−12425.
(32) Morrison, H.; Jernstrom, B.; Nordenskjold, M.; Thor, H.; Orrenius, S. Induction of DNA damage by menadione (2-methyl-1,4-naphthoquinone) in primary cultures of rat hepatocytes. *Biochem. Pharmacol.* **1984**, *33*, 1763−1769.
(33) Han, Y.; Shen, H.; Carr, B. I.; Wipf, P.; Lazo, J. S.; Pan, S. S. NAD(P)H:quinone oxidoreductase-1-dependent and -independent cytotoxicity of potent quinone Cdc25 phosphatase inhibitors. *J. Pharmacol. Exp. Ther.* **2004**, *309*, 64−70.
(34) Irwin, J. J.; Shoichet, B. K. ZINC—a free database of commercially available compounds for virtual screening. *J. Chem. Inf. Model.* **2005**, *45*, 177−182.

(35) *GLIDE*, version 5.7; Schrodinger, LLC: New York, 2011; http://www.schrodinger.com
(36) Jorgensen, W. L. *QikProp, version 3.4*; Schrodinger, LLC: New York, 2011.
(37) *MDL CrossFire Commander*, release version 7.0 SP2; Elsevier MDL: San Ramon, CA; www.mdli.com.
(38) PubChem Compound database available at http://www.ncbi.nlm.nih.gov/sites/entrez/.
(39) Sohn, J.; Kiburz, B.; Li, Z.; Deng, L.; Safi, A.; Pirrung, M. C.; Rudolph, J. Inhibition of Cdc25 phosphatases by indolyldihydroxyquinones. *J. Med. Chem.* **2003**, *46*, 2580−2588.
(40) Brisson, M.; Nguyen, T.; Wipf, P.; Joo, B.; Day, B. W.; Skoko, J. S.; Schreiber, E. M.; Foster, C.; Bansal, P.; Lazo, J. S. Redox regulation of Cdc25B by cell-active quinolinediones. *Mol. Pharmacol.* **2005**, *68*, 1810−1820.
(41) Brisson, M.; Foster, C.; Wipf, P.; Joo, B.; Tomko, R. J., Jr.; Nguyen, T.; Lazo, J. S. Independent mechanistic inhibition of cdc25 phosphatases by a natural product caulibugulone. *Mol. Pharmacol.* **2007**, *71*, 184−192.
(42) Zhou, Y. B.; Feng, X.; Wang, L. N.; Du, J. Q.; Zhou, Y. Y.; Yu, H. P.; Zang, Y.; Li, J. Y.; Li, J. LGH00031, a novel ortho-quinonoid inhibitor of cell division cycle 25B, inhibits human cancer cells via ROS generation. Zhou et al. *Acta Pharmacol. Sin.* **2009**, *30*, 1359−1368.
(43) Hilal, S. H.; Karickhoff, S. W.; Carreira, L. A. Estimation of microscopic, zwitterionic ionization constants, isoelectric point and molecular speciation of organic compounds. *Talanta* **1999**, *50*, 827−840.
(44) Müller, P. A new photoremovable protecting group absorbing above 500 nm: (6-hydroxy-3-ox-3*H*-xanthen-9-yl)methyl and its derivatives. Ph.D. dissertation , University of Basel, December 2007.
(45) McCain, D. F.; Wu, L.; Nickel, P.; Kassack, M. U.; Kreimeyer, A.; Gagliardi, A.; Collins, D. C.; Zhang, Z. Y. Suramin derivatives as inhibitors and activators of protein-tyrosine phosphatases. *J. Biol. Chem.* **2004**, *279*, 14713−14725.
(46) Park, H.; Bahn, Y. J.; Jung, S.-K.; Jeong, D. G.; Lee, S.-H.; Seo, I.; Yoon, T.-S.; Kim, S. J.; Ryu, S. E. Discovery of novel Cdc25 phosphatase inhibitors with micromolar activity based on the structure-based virtual screening. *J. Med. Chem.* **2008**, *51*, 5533−5541.
(47) (a) Johnston, P. A.; Foster, C. A.; Tierno, M. B.; Shun, T. Y.; Shinde, S. N.; Paquette, W. D.; Brummond, K. M.; Wipf, P.; Lazo, J. S. Cdc25B dual-specificity phosphatase inhibitors identified in a high-throughput screen of the NIH compound library. *Assay Drug Dev. Technol.* **2009**, *7*, 250−265. (b) Sun, Y. W.; Huang, W. J.; Hsiao, C. J.; Chen, Y. C.; Lu, P. H.; Guh, J. H. Methoxychalcone induces cell-cycle arrest and apoptosis in human hormone-resistant prostate cancer cells through PI 3-kinase-independent inhibition of mTOR pathways. *Prostate* **2010**, *70*, 1295−1306. (c) Prasad, S.; Kaur, J.; Roy, P.; Kalra, N.; Shukla, Y. Theaflavins induce G2/M arrest by modulating expression of p21waf1/cip1, cdc25C and cyclin B in human prostate carcinoma PC-3 cells. *Life Sci.* **2007**, *81*, 1323−1331.
(48) (a) Chen, R. Q.; Yang, Q. K.; Lu, B. W.; Yi, W.; Cantin, G.; Chen, Y. L.; Fearns, C.; Yates, J. R., III; Lee, J. D. CDC25B mediates rapamycin-induced oncogenic responses in cancer cells. *Cancer Res.* **2009**, *69*, 2663−2668. (b) Wei, F.; Xie, Y.; Tao, L.; Tang, D. Both ERK1 and ERK2 kinases promote G2/M arrest in etoposide-treated MCF7 cells by facilitating ATM activation. *Cell. Signalling* **2010**, *22*, 1783−1789. (c) Brault, L.; Bagrel, D. Activity of novel Cdc25 inhibitors and preliminary evaluation of their potentiation of chemotherapeutic drugs in human breast cancer cells. *Life Sci.* **2008**, *82*, 315−323.
(49) Takagaki, K.; Katsuma, S.; Kaminishi, Y.; Horio, T.; Tanaka, T.; Ohgi, T.; Yano, J. Role of Chk1 and Chk2 in Ara-C-induced differentiation of human leukemia K562 cells. *Genes Cells* **2005**, *10*, 97−106.
(50) Brisson, M.; Nguyen, T.; Vogt, A.; Yalowich, J.; Giorgianni, A.; Tobi, D.; Bahar, I.; Stephenson, C. R.; Wipf, P.; Lazo, J. S. Discovery and characterization of novel small molecule inhibitors of human Cdc25B dual specificity phosphatase. *Mol. Pharmacol.* **2004**, *66*, 824−833.
(51) Li, C.; Xu, L.; Wolan, D. W.; Wilson, I. A.; Olson, A. J. Virtual screening of human 5-aminoimidazole-4-carboxamide ribonucleotide transformylase against the NCI diversity set by use of AutoDock to identify novel nonfolate inhibitors. *J. Med. Chem.* **2004**, *47*, 6681−6690.
(52) (a) Contour-Galcera, M. O.; Sidhu, A.; Prévost, G.; Bigg, D.; Ducommun, B. What's new on CDC25 phosphatase inhibitors. *Pharmacol. Ther.* **2006**, *115*, 1−12. (b) Jiang, Z. X.; Zhang, Z. Y. Targeting PTPs with small molecule inhibitors in cancer treatment. *Cancer Metastasis Rev.* **2008**, *27*, 263−272.
(53) Keinan, S.; Paquette, W. D.; Skoko, J. J.; Beratan, D. N.; Yang, W.; Shinde, S.; Johnston, P. A.; Lazo, J. S.; Wipf, P. Computational design, synthesis and biological evaluation of para-quinone based inhibitors for redox regulation of the dual-specificity phosphatase Cdc25B. *Org. Biomol. Chem.* **2008**, *6*, 3256−3263.
(54) *QikProp*, version 3.4; Schrödinger LLC: New York, 2011.
(55) Artursson, P.; Karlsson, J. Correlation between oral drug absorption in humans and apparent drug permeability coefficients in human intestinal epithelial (Caco-2) cells. *Biochem. Biophys. Res. Commun.* **1991**, *175*, 880−885.
(56) Berman, H. M.; Westbrook, J.; Feng, Z.; Gilliland, G.; Bhat, T. N.; Weissig, H.; Shindyalov, I. N.; Bourne, P. E. The Protein Data Bank. *Nucleic Acids Res.* **2000**, *28*, 235−242.
(57) Buhrman, G.; Parker, B.; Sohn, J.; Rudolph, J.; Mattos, C. Structural mechanism of oxidative regulation of the phosphatase Cdc25B via an intramolecular disulfide bond. *Biochemistry* **2005**, *44*, 5307−5316.
(58) Taylor, N. R.; Borhani, D.; Epstein, D.; Rudolph, J.; Ritter, K.; Fujimori, T.; Robinson, S.; Eckstein, J.; Haupt, A.; Walker, N.; Dixon, R.; Choquette, D.; Blanchard, J.; Kluge, A.; Pal, K.; Bockovich, N.; Come, J.; Hediger, M. Crystal structure of CDC25 proteins and its use in rational design of inhibitors. Patent WO 2001/16300 A2, 2001.
(59) *Maestro*, version 9.2; Schrödinger LLC: New York, 2011.
(60) Jorgensen, W. L.; Maxwell, D. S.; Tirado-Rives, J. Development and testing of the OPLS all-atom force field on conformational energetics and properties of organic liquids. *J. Am. Chem. Soc.* **1996**, *118*, 11225−11236.
(61) Lipinski, C. A.; Lombardo, F.; Dominy, B. W.; Feeney, P. J. Experimental and computational approaches to estimate solubility and permeability in drug discovery and development settings. *Adv. Drug Delivery Rev.* **2001**, *46*, 3−26.
(62) Friesner, R. A.; Banks, J. L.; Murphy, R. B.; Halgren, T. A.; Klicic, J. J.; Mainz, D. T.; Repasky, M. P.; Knoll, E. H.; Shelley, M.; Perry, J. K.; Shaw, D. E.; Francis, P.; Shenkin, P. S. GLIDE: a new approach for rapid, accurate docking and scoring. 1. Method and assessment of docking accuracy. *J. Med. Chem.* **2004**, *47*, 1739−1749.
(63) Friesner, R. A.; Murphy, R. B.; Repasky, M. P.; Frye, L. L.; Greenwood, J. R.; Halgren, T. A.; Sanschagrin, P. C.; Mainz, D. T. Extra precision Glide: docking and scoring incorporating a model of hydrophobic enclosure for protein-ligand complexes. *J. Med. Chem.* **2006**, *49*, 6177−6196.
(64) *Jaguar*, version 7.8; Schrödinger, LLC: New York, 2011.
(65) Zhao, Y.; Truhlar, D. G. The M06 suite of density functionals for main group thermochemistry, thermochemical kinetics, noncovalent interactions, excited states, and transition elements: two new functionals and systematic testing of four M06-class functionals and 12 other functionals. *Theor. Chem. Acc.* **2008**, *120*, 215−241.
(66) (a) Rogstad, K. N.; Jang, Y. H.; Sowers, L. C.; Goddard, W. A., III. First principles calculations of the pK_a values and tautomers of isoguanine and xanthine. *Chem. Res. Toxicol.* **2003**, *16*, 1455−1462. (b) Jang, Y. H.; Goddard, W. A., III; Noyes, K. T.; Sowers, L. C.; Hwang, S.; Chung, D. S. pK_a values of guanine in water: density functional theory calculations combined with Poisson−Boltzmann continuum-solvation model. *J. Phys. Chem. B* **2003**, *107*, 344−357. (c) Hwang, S.; Jang, Y. H.; Chung, D. S. Gas phase proton affinity, basicity, and pK(a) values for nitrogen containing heterocyclic aromatic compounds. *Bull. Korean Chem. Soc.* **2005**, *26*, 585−588.
(67) Tannor, D. J.; Marten, B.; Murphy, R.; Friesner, R. A.; Sitkoff, D.; Nicholls, A.; Ringnalda, M.; Goddard, W. A., III; Honig, B.

Accurate first principles calculation of molecular charge distributions and solvation energies from ab initio quantum mechanics and continuum dielectric theory. *J. Am. Chem. Soc.* **1994**, *116*, 11875−11882.
(68) Marten, B.; Kim, K.; Cortis, C.; Friesner, A.; Murphy, R. B.; Ringnalda, M. N.; Sitkoff, D.; Honig, B. New model for calculation of solvation free energies: correction of self-consistent reaction field continuum dielectric theory for short-range hydrogen-bonding effects. *J. Phys. Chem.* **1996**, *100*, 11775−11788.
(69) Ihlenfeldt, W. D.; Voigt, J. H.; Bienfait, B.; Oellien, F.; Nicklaus, M. C. Enhanced CACTVS browser of the Open NCI Database. *J. Chem. Inf. Comput. Sci.* **2002**, *42*, 46−57.
(70) Willett, P. Similarity-based approaches to virtual screening. *Biochem. Soc. Trans.* **2003**, *31*, 603−606.
(71) Martin, Y. C.; Kofron, J. L.; Traphagen, L. M. Do structurally similar molecules have similar biological activity? *J. Med. Chem.* **2002**, *45*, 4350−4358.
(72) Bhattacharjee, H.; Sheng, J.; Ajees, A. A.; Mukhopadhyay, R.; Rosen, B. P. Adventitious arsenate reductase activity of the catalytic domain of the human Cdc25B and Cdc25C phosphatases. *Biochemistry* **2010**, *49*, 802−809.
(73) Cory, A. H.; Owen, T. C.; Barltrop, J. A.; Cory, J. G. Use of an aqueous soluble tetrazolium/formazan assay for cell growth assays in culture. *Cancer Commun.* **1991**, *3*, 207−212.
(74) Chiaviello, A.; Paciello, I.; Postiglione, I.; Crescenzi, E.; Palumbo, G. Combination of photodynamic therapy with aspirin in human-derived lung adenocarcinoma cells affects proteasome activity and induces apoptosis. *Cell Proliferation* **2010**, *43*, 480−493.